Solution Structure and Dynamics of Ras p21·GDP Determined by Heteronuclear Three- and Four-Dimensional NMR Spectroscopy†,‡

Per J. Kraulis,§,‖ Peter J. Domaille,⊥ Sharon L. Campbell-Burk,⊥,# Thomas Van Aken,⊥ and Ernest D. Laue*,§

Department of Biochemistry, Cambridge Centre for Molecular Recognition, University of Cambridge, Tennis Court Road, Cambridge CB2 1QW, U.K., and DuPont Merck Pharmaceutical Company, P.O. Box 80328, Wilmington, Delaware 19880-0328

Received October 19, 1993; Revised Manuscript Received December 21, 1993®

ABSTRACT: A high-resolution solution structure of the GDP form of a truncated version of the ras p21 protein (residues 1–166) has been determined using NMR spectroscopy. Ras p21 is the product of the human *ras* protooncogene and a member of a ubiquitous eukaryotic gene family which is highly conserved in evolution. A virtually complete assignment (^{13}C, ^{15}N, and ^{1}H), including stereospecific assignments of 54 C_β methylene protons and 10 C_γ methyl protons of valine residues, was obtained by analysis of three- and four-dimensional (3D and 4D) heteronuclear NMR spectra using a newly developed 3D/4D version of the ANSIG software. A total of 40 converged structures were computed from 3369 experimental restraints consisting of 3167 nuclear Overhauser effect (NOE) derived distances, 14 ϕ and 54 χ_1 torsion angle restraints, 109 hydrogen bond distance restraints, and an additional 25 restraints derived from literature data defining interactions between the GDP ligand, the magnesium ion, and the protein. The structure in the region of residues 58–66 (loop L4), and to a lesser degree residues 30–38 (loop L2), is ill-defined. Analysis of the dynamics of the backbone ^{15}N nuclei in the protein showed that residues within the regions 58–66, 107–109, and, to a lesser degree, 30–38 are dynamically mobile on the nanosecond time scale. The root mean square (rms) deviations between the 40 solution structures and the mean atomic coordinates are 0.78 Å for the backbone heavy atoms and 1.29 Å for all non-hydrogen atoms if all residues (1–166) are included in the analysis. If residues 30–38 and residues 58–66 are excluded from the analysis, the rms deviations are reduced to 0.55 and 1.00 Å, respectively. The structure was compared to the most highly refined X-ray crystal structure of ras p21·GDP (1–189) [Milburn, M. V., Tong, L., de Vos, A. M., Brünger, A. T., Yamaizumi, Z., Nishimura, S., & Kim, S.-H. (1990) *Science 24*, 939–945]. The structures are very similar except in the regions found to be mobile by NMR spectroscopy. In addition, the second α-helix (helix-2) has a slightly different orientation. The rms deviation between the average of the solution structures and the X-ray crystal structure is 0.94 Å for the backbone heavy atoms if residues 31–37 and residues 59–73 are excluded from the analysis.

The ras proteins are highly conserved 21-kDa (p21) guanine nucleotide binding proteins which play a critical role in the control of cellular growth by cycling between the biologically active GTP[1] and inactive GDP forms of the protein; they have a low intrinsic GTPase activity and are members of a GTPase superfamily. Their activity is enhanced by guanine nucleotide exchange factors (GEFs) that promote dissociation of GDP and thereby allow GTP to bind and activate the protein. Downregulation is accomplished by GTPase activating proteins (GAPs) that bind and speed up the intrinsic rate of GTP hydrolysis so inactivating the protein [for a review, see Bourne *et al.* (1991)]. Mutations to *ras* genes are very widespread in human tumors, emphasizing the important role these proteins play in controlling normal cell growth (Barbacid, 1987; Bos, 1989); these mutations have been found to involve a small set of residues, mainly Gly-12, Gly-13, and Gln-61.

In the last year or so, remarkable progress has been made in understanding how ras proteins couple events that occur at the cell surface to changes in gene expression in the nucleus. Several groups have shown that receptors with intrinsic tyrosine kinase activity, e.g., the EGF receptor, when activated, phosphorylate themselves and promote binding of an adaptor protein, a so-called SH3–SH2–SH3 domain protein (SH stands for homology to a domain in the Src tyrosine kinase), via the SH2 domain. The SH3 domains of these adaptor proteins appear to bind GEFs, and they therefore couple the GEF to the inner surface of the plasma membrane where the ras proteins are anchored (Simon *et al.*, 1993; Olivier *et al.*, 1993; Egan *et al.*, 1993; Rozakis-Adcock *et al.*, 1993; Li *et al.*, 1993; Gale *et al.*, 1993; Buday & Downward, 1993; Chardin *et al.*, 1993). The insulin receptor has also been shown to activate ras via phosphorylation of Shc which in turn promotes binding of the adaptor protein (Baltensperger *et al.*, 1993; Skolnik *et al.*, 1993). More recently, researchers have demonstrated a link between ras proteins and the mitogen-activated protein kinases (MAPs). These kinases appear to

† At Cambridge this work was supported by the Science and Engineering Research Council (SERC) and by Meiko Ltd. P.J.K. thanks the Swedish Natural Science Research Council for a postdoctoral fellowship.

‡ Coordinates have been deposited in the Brookhaven Protein Data Bank [codes 1CRQ (SA_{av}) and 1CRP and 1CRR (final structures 1–20 and 21–40, respectively)].

* Author to whom correspondence should be addressed.

§ Cambridge Centre for Molecular Recognition.

‖ Present address: Centre for Structural Biochemistry, Karolinska Institute, NOVUM, S-141, 57 Huddinge, Sweden.

⊥ DuPont Merck Pharmaceutical Co.

Present address: Department of Biochemistry and Biophysics, University of North Carolina, Chapel Hill, NC 27599-7260.

® Abstract published in *Advance ACS Abstracts,* February 15, 1994.

[1] Abbreviations: GDP, guanosine 5′-diphosphate; GTP, guanosine 5′-triphosphate; GDPCP, β,γ-methylene derivative of GTP; GPPNP, β,γ-imido derivative of GTP; NMR, nuclear magnetic resonance; 2D, 3D, and 4D, two, three, and four dimensional, respectively; Tris, tris(hydroxymethyl)aminomethane; DTT, dithiothreitol; PMSF, phenylmethanesulfonyl fluoride; EDTA, ethylenediaminetetraacetic acid; BSA, bovine serum albumin; ADP, adenosine 5′-diphosphate; NOESY, NOE spectroscopy; TOCSY, total correlation spectroscopy; COSY, correlated spectroscopy; HSQC, heteronuclear single-quantum correlation.

0006-2960/94/0433-3515$04.50/0

regulate the activity of various transcription factors (Davis, 1993). In addition, the Raf-1 protein, itself a protein kinase, has been shown to phosphorylate and activate the MAP kinase kinase (or MEK) (Kyriakis *et al.*, 1992; Howe *et al.*, 1992; Dent *et al.*, 1992). Now the most recent work has demonstrated that the ras proteins and Raf-1 associate when ras is in its active GTP form (Moodie *et al.*, 1993; Zhang, *et al.*, 1993; Warne *et al.*, 1993; Van Aelst *et al.*, 1993; Vojtek *et al.*, 1993). It was also possible to demonstrate that MEK associates with the complex (Moodie *et al.*, 1993), perhaps being directly phosphorylated by Raf-1 (Hughes *et al.*, 1993). Although Raf-1 may turn out not to be the only direct "downstream effector" of ras, for the first time there is now no obvious gap in the pathway from events that occur at the plasma membrane to changes in gene transcription in the nucleus.

Several high-resolution crystal structures of ras proteins complexed with either GDP or stable GTP analogues have been solved in recent years (De Vos *et al.*, 1988; Tong *et al.*, 1989, 1991; Pai *et al.*, 1989, 1990; Brünger *et al.*, 1990; Milburn *et al.*, 1990; Krengel *et al.*, 1990). In addition, an elegant time-resolved X-ray crystallographic study of the conformational change in ras p21 undergoing GTP hydrolysis has been presented (Schlichting *et al.*, 1990a). However, when a protein switches between different, energetically finely balanced conformational states, crystal packing forces are more likely to influence the structure. For example, in the crystal structure of the complex of GDPCP (a GTP analogue) and ras p21 (1–171) (Brünger *et al.*, 1990; Milburn *et al.*, 1990), the four crystallographically independent molecules have different conformations in both loop L2 and loop L4 (regions 30–37 and 60–66, respectively). Furthermore, at present there is no structural information available as to how ras proteins interact with proteins which modulate their activity [e.g., GEFs (Martegani *et al.*, 1992; Shou *et al.*, 1992; Wei *et al.*, 1992; Bowtell *et al.*, 1992; Kikuchi *et al.*, 1992) or GAPs (Trahey & McCormick, 1987; Gibbs *et al.*, 1988; Martin *et al.*, 1990; Xu *et al.*, 1990; Ballester *et al.*, 1990)]. Detailed studies using NMR spectroscopy may therefore be useful for probing the solution structure and dynamics of ras proteins and their interactions with either GEFs, GAPs, or downstream effectors such as Raf-1.

Furthermore, despite the intensive structural and biochemical studies, the mechanism by which ras proteins hydrolyze GTP is still unclear. Two distinct mechanisms of GTP hydrolysis have been proposed on the basis of X-ray diffraction studies. In the first, Pai *et al.* (1990) proposed that a water molecule is involved in a nucleophilic attack on the γ-phosphate of GTP where Gln-61 acts as a general base to abstract a proton from the attacking water molecule. Prive *et al.* (1992) instead proposed that Gln-61 directly stabilizes the transition state in the hydrolysis reaction. However, it must be pointed out that these predictions were tentative as definitive structural information was lacking because the catalytic loop L4, in which Gln-61 is located, is poorly defined in the structures determined by X-ray diffraction methods. More recently, biochemical and theoretical studies have suggested that neither mechanism is in fact likely. In an elegant study, Chung *et al.* (1993) replaced Gln-61 by the isosteric nitro analogue and found that the intrinsic rate of GTP hydrolysis and its activation by GAP was only slightly altered. The nitro group is a much poorer base, suggesting that Gln-61 does not act as a base to catalyze the reaction. Furthermore, the nitro group would not act as a hydrogen bond donor and is a weak hydrogen bond acceptor, arguing against a role for Gln-61 in stabilizing the transition state. In addition, free energy perturbation calculations also suggest that it is unlikely that Gln-61 acts as a general base (Langen *et al.*, 1992). Again, NMR studies of the structure and the dynamics of ras have the potential to provide insight into the mechanism of GTP hydrolysis and may aid in understanding differences between the wild-type and oncogenic proteins.

Previous NMR studies of ras p21·GDP, in which specifically labeled amino acids (^{15}N, ^{13}C, and ^{2}H) had been incorporated, allowed some assignments to amino acid *type* (Campbell-Burk *et al.*, 1989; Campbell-Burk, 1989; Redfield & Papastavros, 1990; Yamasaki *et al.*, 1989; Schlichting *et al.*, 1990b). Our initial attempts to assign ras p21·GDP using the intact protein (189 residues) were plagued by problems of sample instability, probably resulting from aggregation due to oxidation of cysteine(s) in the carboxy-terminal region of the protein. Light scattering data showed that at the concentrations required for NMR studies the intact protein forms oligomers whereas a truncated form, residues 1–166, appeared to be monomeric. $^{1}H_N$ and ^{15}N chemical shifts of glycine residues in the guanine nucleotide binding domain were found to be very similar in the two forms of the protein, consistent with their similar biochemical properties (John *et al.*, 1989). We have therefore used ras p21 (1–166) for all our NMR studies.

We and others have previously reported the complete assignment of the backbone nuclei (^{13}C, ^{15}N, and ^{1}H) in the GDP form of the protein (Campbell-Burk *et al.*, 1992; Yamasaki *et al.*, 1992; Muto *et al.*, 1993). In this paper we present a high-resolution three-dimensional structure and studies of the dynamics of the GDP form of the protein in solution. The structure was generated from a total of 3369 experimental restraints derived from 2D homonuclear and 3D/4D heteronuclear NOE data, heteronuclear and homonuclear coupling constants obtained from multidimensional NMR spectra, and amide exchange studies. The dynamics of the protein were studied by analysis of heteronuclear NOE and T_1 and T_2 measurements of a ^{15}N-labeled protein. The analysis of all the NMR spectra and the compilation of the structural data were greatly facilitated by the development of a 3D/4D version of the interactive computer graphics assignment program ANSIG which we briefly describe (Kraulis, 1989; Kraulis *et al.*, unpublished work). The solution structure and dynamics were compared to the structures of the GDP form of the protein determined by X-ray diffraction methods.

MATERIALS AND METHODS

Protein Expression and Cell Growth. The *Escherichia coli* expression vectors pAT-rasH (Der *et al.*, 1986a) and pTACCrasC′ (John *et al.*, 1989), encoding the first 166 residues of the human ras p21 protein [ras p21 (1–166)], were kindly provided by Professor C. Der and Professor A. Wittinghofer, respectively. The plasmids were transformed into *E. coli* strain JM105. Uniformly enriched ^{15}N and $^{13}C/^{15}N$ samples were obtained by growing bacteria at 33 °C on either $(^{15}NH_4)_2SO_4$ as the sole nitrogen source or [$^{13}C_6$]-glucose/$(^{15}NH_4)_2SO_4$ as the sole carbon and nitrogen sources, respectively. At a turbidity of ~2.3 OD (600 nm), expression of the protein was induced by the addition of 1 mM isopropyl β-D-thiogalactoside. Samples were collected hourly, and the fermenter was chilled when the glucose concentration fell to zero (~4 h). The cells were then harvested and stored at −80 °C.

Protein Purification. All the procedures described below were performed at 4 °C. The cells were washed once, pelleted

at 18000*g* for 20 min, and resuspended to 0.1 g of cell paste/mL with sonication buffer (20 mM Tris-HCl, pH 7.2, 100 mM NaCl, 5 mM $MgCl_2$, 1 mM DTT, and 1 mM PMSF). The cells were then broken by sonication in a 250-mL Rossett cup at maximum output using a pulsed 50% duty cycle for three 15-min periods (separated by 10 min) in a Heat Systems W-375 sonicator equipped with a $^1/_2$-in. button tip. The soluble and insoluble fractions were separated by centrifugation at 18000*g* for 30 min. The resultant pellet containing inclusion bodies was resuspended to 10 mg of protein/mL with solubilization buffer (5.0 M guanidine hydrochloride, 50 mM Tris-HCl, pH 8.0, 50 mM NaCl, 5 mM $MgCl_2$, 1 mM EDTA, 1 mM DTT, 1 mM PMSF, and 30 μM GDP) and stirred for 1 h. The insoluble material was pelleted by centrifugation at 17000*g* for 30 min, and the supernatant was diluted 100-fold with dilution buffer (solubilization buffer without the guanidine hydrochloride) to give a final protein concentration of 100 μg/mL. The diluted solubilized protein was incubated without stirring for a further 2 h. The sample was then dialyzed for 4 h and then overnight against 2 volumes of dialysis buffer (20 mM Tris-HCl, pH 8.0, 5 mM $MgCl_2$, 1 mM DTT, 1 mM PMSF, 5% glycerol, and 30 μM GDP). In the morning the dialyzed material was loaded onto a Q Sepharose Fast Flow (Pharmacia) anion-exchange column (4.4 × 14.5 cm) pre-equilibrated with dialysis buffer containing 10 mM NaCl at a flow rate of 480 mL h^{-1}. The protein was eluted using a 2-L 10–300 mM NaCl gradient. The fractions were analyzed using 10–20% polyacrylamide gel electrophoresis, and those containing the protein were pooled and concentrated using a YM10 membrane in an Amicon-stirred cell to >20 mg mL^{-1} and stored at −20 °C in 50% glycerol. The Bio-Rad protein assay (Bradford, 1976) was used to determine protein concentrations using bovine serum albumin (BSA, Sigma A-7906) as the standard.

GDP Binding Assays. ^{3}H-Labeled GDP binding to ras p21 (1–166) was measured using a filter binding assay. The protein solution (100 μL, ~12.5 pmol) was incubated at 37 °C with 80 mM Tris–maleate, pH 7.5, 5 mM $MgCl_2$, 50 mM NaCl, 1 mM DTT, 0.5 mg/mL BSA, 16 μM ADP, and 8 μM [8-^{3}H]-GDP (1950 cpm/pmol). After 24 h of incubation, a 40-μL aliquot (approximately 5 pmol of protein) was placed onto a Schleicher & Schuell BA85 nitrocellulose filter disk (25-mm diameter) premoistened with assay buffer (80 mM Tris–maleate, pH 7.5, 5 mM $MgCl_2$, 50 mM NaCl, and 1 mM DTT). The disks were washed once with 10 mL of ice-cold assay buffer, followed by a second 5 mL, before being placed in scintillation vials and dissolved in 10 mL of Filtron-X (National Diagnostics) scintillation cocktail for 24 h and then counted.

Preparation of Protein Samples for NMR Spectroscopy. Protein samples (~800 μL) were loaded onto a PD-10 G25 column (Pharmacia) previously equilibrated with NMR buffer [either 90% H_2O/10% D_2O or 100% D_2O containing 20 mM Tris–maleate-d_{15}, pH (or pD) 6.5, 40 mM NaCl, 5 mM $MgCl_2$, 5 mM DTT, 0.01% sodium azide, and 30 μM GDP] and then eluted with the same buffer (~1.6 mL). They were concentrated to ~500 μL in a Centricon-10 (Amicon); for the 100% D_2O samples the protein was typically washed and reconcentrated 3 times using 1.5 mL of the 100% D_2O NMR buffer.

NMR Spectroscopy. All NMR experiments were recorded under identical conditions on ~1.5 mM samples of ras p21 (1–166)·GDP, either unlabeled or uniformly labeled (>90%) with ^{15}N or ^{13}C/^{15}N, at 30 °C on a Bruker AMX600 NMR spectrometer. The 4D HCANNH and HCA(CO)NNH spectra were acquired and processed as discussed previously (Campbell-Burk *et al.*, 1992).

2D NOESY and *z*-filtered TOCSY (Rance, 1987) spectra were acquired, with 256 (t_1) × 1024 (t_2) complex points to give acquisition times of 31.7 and 127.0 ms in t_1 and t_2, respectively, on the unlabeled protein sample in 100% D_2O. The NOESY spectra were acquired with mixing times of 70 and 100 ms while the TOCSY spectrum was acquired using a DIPSI-2 (Shaka *et al.*, 1988) mixing time of 46 ms.

3D ^{15}N-edited NOESY and TOCSY spectra (Marion *et al.*, 1989a,b) and the 4D ^{13}C/^{15}N-edited NOESY spectrum (Kay *et al.*, 1990) were acquired with mixing times of 100 ms (NOESY) and 35 ms (TOCSY) on either the ^{15}N-labeled or the ^{13}C/^{15}N-labeled protein in 90% H_2O/10% D_2O. The 3D ^{15}N-edited spectra were acquired with a total of 128 (t_1) × 32 (t_2) × 512 (t_3) complex points to give acquisition times of 15.9, 32.0, and 63.5 ms in t_1, t_2, and t_3, respectively. The 4D ^{13}C/^{15}N-edited NOESY spectrum was acquired with a total of 64 (t_1) × 16 (t_2) × 8 (t_3) × 512 (t_4) complex points to give acquisition times of 10.2, 4.8, 8.0, and 63.5 ms in t_1, t_2, t_3, and t_4, respectively. 2D ^{1}H–^{15}N HSQC spectra to measure heteronuclear NOEs and T_1s and T_2s were recorded, on the ^{15}N-labeled sample, essentially as described by Barbato *et al.* (1992); spectra were acquired with a total of 64 (t_1) × 512 (t_2) complex points to give acquisition times of 64.0 and 63.5 ms in t_1 and t_2, respectively.

3D ^{13}C-edited HCCH-COSY, HCCH-TOCSY (Bax *et al.*, 1990a,b), and NOESY (Ikura *et al.*, 1990; Zuiderweg *et al.*, 1990) spectra were acquired on the ^{13}C/^{15}N-labeled protein in 100% D_2O. The HCCH-COSY and TOCSY spectra (24-ms mixing time) were acquired with a total of 80 (t_1) × 32 (t_2) × 512 (t_3) complex points to give acquisition times of 9.9, 9.6, and 63.5 ms in t_1, t_2, and t_3, respectively. The NOESY spectrum (100-ms mixing time) was acquired with a total of 128 (t_1) × 26 (t_2) × 256 (t_3) complex points to give acquisition times of 19.2, 6.5, and 31.7 ms in t_1, t_2, and t_3, respectively. 3D SOFT HCCH-COSY and SOFT HCCH-E.COSY spectra (for the stereospecific assignment of the ^{1}Hβ protons and determination of the χ_1 torsion angle restraints) (Eggenberger *et al.*, 1992) were acquired with a total of 32 (t_1) × 140 (t_2) × 512 (t_3) complex points to give acquisition times of 6.4, 14.0, and 63.5 ms in t_1, t_2, and t_3, respectively.

The ^{1}H carrier was in all cases positioned on the water resonance whose intensity, in the spectra recorded in 90% H_2O/10% D_2O, was reduced by presaturation (20–25-Hz radio-frequency field strength) and baseline correction in the t_3 (for 3D NMR spectra) or t_4 (for 4D NMR spectra) time domain (Marion *et al.*, 1989c). 3D and 4D NMR spectra were typically first processed using conventional Fourier transforms in t_3 (3D) or t_4 and t_3 (4D), respectively; for the 3D ^{15}N-edited NOESY and TOCSY spectra and the 4D ^{13}C/^{15}N-edited NOESY spectrum, the low-frequency portion of the spectrum was discarded after the first transform. Processing in the t_1 and t_2 dimensions was typically achieved using a two-dimensional maximum entropy algorithm (Laue *et al.*, 1986). All spectra were analyzed using a 3D/4D version of the ANSIG program running on a Silicon Graphics Indigo computer (Kraulis, 1989; Kraulis *et al.*, unpublished results).

Structures were calculated from the experimental constraints using the program X-PLOR (Brünger, 1992), employing either the full simulated annealing (SA) protocol which starts from an extended strand [Nilges *et al.*, 1988; sa.inp, Nilges in Brünger (1992)] or a shortened version which starts from a structure where the main chain is already close to the

final fold. All calculations were performed on Silicon Graphics Indigo computers.

RESULTS AND DISCUSSION

Assignment of the NMR Spectra: General Considerations. We have previously reported the sequential assignment of the backbone nuclei (^{13}C, ^{15}N, and ^{1}H) using a novel 4D NMR strategy (Campbell-Burk *et al.*, 1992). In order to extend this assignment to include the side-chain resonances using ANSIG, and also so that we could develop the 3D/4D version of the software, we had to repeat this assignment. In so doing, the relevant assignments were entered into the internal database within the program, where they were later used in compiling the restraints list for the structure calculations (see Analysis of the NOESY Spectra, below). The assignment was carried out sequentially, assigning as far as possible all the resonances for each residue, in turn, as we worked through the sequence of the protein. Although the assignment of the backbone and side-chain resonances could have been done separately, the ease with which we can move between the different spectra using ANSIG favored a simultaneous assignment of all the resonances in a particular residue; in many cases it allowed us to check unambiguously that we had the correct residue type at each position in the sequence. Most residues could be completely assigned using a combination of the HCANNH and HCA(CO)NNH 4D NMR spectra for the backbone resonances (Boucher *et al.*, 1992a,b) and the 3D HCCH-COSY and TOCSY spectra for the side-chain resonances (Bax *et al.*, 1990a,b). Assignment of the aromatic side chains and proline residues, which lack amide protons and therefore do not appear in the two 4D NMR spectra, required in addition the 4D $^{13}C/^{15}N$-edited and 3D ^{13}C-edited NOESY spectra (Kay *et al.*, 1990; Ikura *et al.*, 1990; Zuiderweg *et al.*, 1990), while glycine residues, which also do not appear in the 4D HCANNH and HCA(CO)NNH spectra, required in addition the 3D ^{15}N-edited NOESY and TOCSY spectra (Marion *et al.*, 1989a,b).

Assignment of the Aliphatic Residues Excluding Glycine and Proline. The 4D HCANNH and HCA(CO)NNH spectra together allowed us to assign the majority of the backbone resonances. Cross peaks correlating the $^{1}H_{\alpha}$, $^{13}C_{\alpha}$, $^{1}H_{N}$, and ^{15}N backbone resonances within a residue and sometimes, in addition, the $^{1}H_{\alpha}$ and $^{13}C_{\alpha}$ resonances in one residue and the $^{1}H_{N}$ and ^{15}N resonances of the C-terminal residue are found in the HCANNH spectrum; by contrast only the latter interresidue cross peaks are found in the HCA(CO)NNH spectrum. The HCA(CO)NNH experiment allows one to distinguish them from the intraresidue cross peaks in the HCANNH spectrum. Additionally, the HCA(CO)NNH experiment detects the interresidue cross peaks with higher sensitivity than the HCANNH experiment. The HCCH-COSY and TOCSY spectra were used to identify the residue type (where possible) and to assign the side-chain resonances. In these spectra cross peaks correlating a directly bonded pair of ^{1}H and ^{13}C nuclei with other protons, either attached to a directly bonded ^{13}C nucleus (HCCH-COSY) or to ^{13}C nuclei further removed (HCCH-TOCSY), are detected.

Figure 1 illustrates the manner in which we used ANSIG to make the assignments. The program displays spectra in multiple windows with 2D planes from either one or several spectra overlaid with each other. On the right-hand edge of each window, there are two scroll bars which, in a 4D NMR spectrum, control the extent of the other two chemical shift ranges that are observed in the window. Essentially in real time the spectrum can be scrolled with the chemical shift range adjusted so that we observe anything between the whole 4D NMR spectrum projected onto a 2D plane or just a single plane from the entire spectrum; in a 3D NMR spectrum only one of the scroll bars is active. In Figure 1a, the overlaid 2D $^{1}H_{N}$–^{15}N planes, at the $^{1}H_{\alpha}$ and $^{13}C_{\alpha}$ chemical shifts of Val-125, from the HCANNH and HCA(CO)NNH 4D NMR spectra are displayed. When the equivalent planes from the HCANNH (green) and the HCA(CO)NNH (magenta) spectra are overlaid, the intraresidue and interresidue cross peaks are immediately identified. As soon as we identify, and label, a cross peak in one of the spectra, its chemical shifts are automatically entered into the database within the program; the assignments in equivalent spectra are also automatically updated.

Many of the 3D and 4D NMR spectra that we recorded were aliased in one or more dimensions. In ANSIG it is possible to correct the chemical shift or a cross peak to account for aliasing. In the ^{15}N dimension, aliasing was resolved by reference to either the 2D ^{1}H–^{15}N HSQC or 4D $^{13}C/^{15}N$-edited NOESY spectra. These spectra were recorded so that cross peaks aliased an even number of times were positive while those aliased an odd number of times were negative (Bax *et al.*, 1991). For the ^{13}C resonances, aliasing of cross peaks was resolved by comparison of the chemical shift with a dictionary of the expected chemical shift ranges for all residue types, based on previous complete assignments of $^{13}C/^{15}N$-labeled proteins [see, e.g., Clore *et al.* (1990)]. Occasionally, we checked the aliasing in spectra recorded with different spectral widths.

A particularly powerful facility in the ANSIG program is the ability to execute macros (i.e., a series of commands) for a given cross peak. For example, by clicking on a button, such a macro was used to display the appropriate orthogonal 2D $^{1}H_{\alpha}$–$^{13}C_{\alpha}$ planes for a given intraresidue cross peak (see Figure 1a,b). This allowed us to check that the two cross peaks do indeed correspond to the intra- and interresidue cross peaks for Val-125, i.e., that the two cross peaks have identical $^{1}H_{\alpha}$ and $^{13}C\alpha$ chemical shifts; it also allowed us to determine those shifts accurately. Having done this, we next displayed, by running a different macro, the overlaid 2D ^{1}H–^{1}H planes, at the appropriate $^{13}C_{\alpha}$ chemical shift, from the HCCH-COSY (orange) and the HCCH-TOCSY (light blue) spectra (see Figure 1c). Here we see the $^{1}H_{\beta}$ (COSY) as well as the $^{1}H_{\beta}$ and $^{1}H_{\gamma}$ (TOCSY) cross peaks characteristic of a valine residue. Knowing the $^{1}H_{\alpha}$ and $^{1}H_{\beta}$ shifts, we next used a further macro to display all the contours at the appropriate $^{1}H_{\alpha}$ and $^{1}H_{\beta}$ shift to find the symmetry-related peak which will be at the $^{13}C_{\beta}$ chemical shift. Once the $^{13}C_{\beta}$ chemical shift had been determined, we were able to display the plane containing cross peaks which identify correlations with the $^{1}H_{\beta}/^{13}C_{\beta}$ nuclei (see Figure 1d). The whole procedure was then repeated to locate the $^{13}C_{\gamma}$ chemical shifts and so on (see Figure 1c); by displaying all the resulting strips from the HCCH spectra, we can confirm that all the expected cross peaks can be seen and therefore that the side-chain type and assignments are correct. In general, this procedure worked very well, and we were able to completely assign some 10 residues per day. However, for some residues it was not sufficient. A few residues were only completed when everything else had been assigned, and in particular, the aromatic, glycine, and proline residues required a different strategy.

Assignment of the Aromatic Residues. The HCCH spectra cannot be used for a complete assignment of aromatic side-chain resonances because the $^{13}C_{\gamma}$ nuclei do not have directly

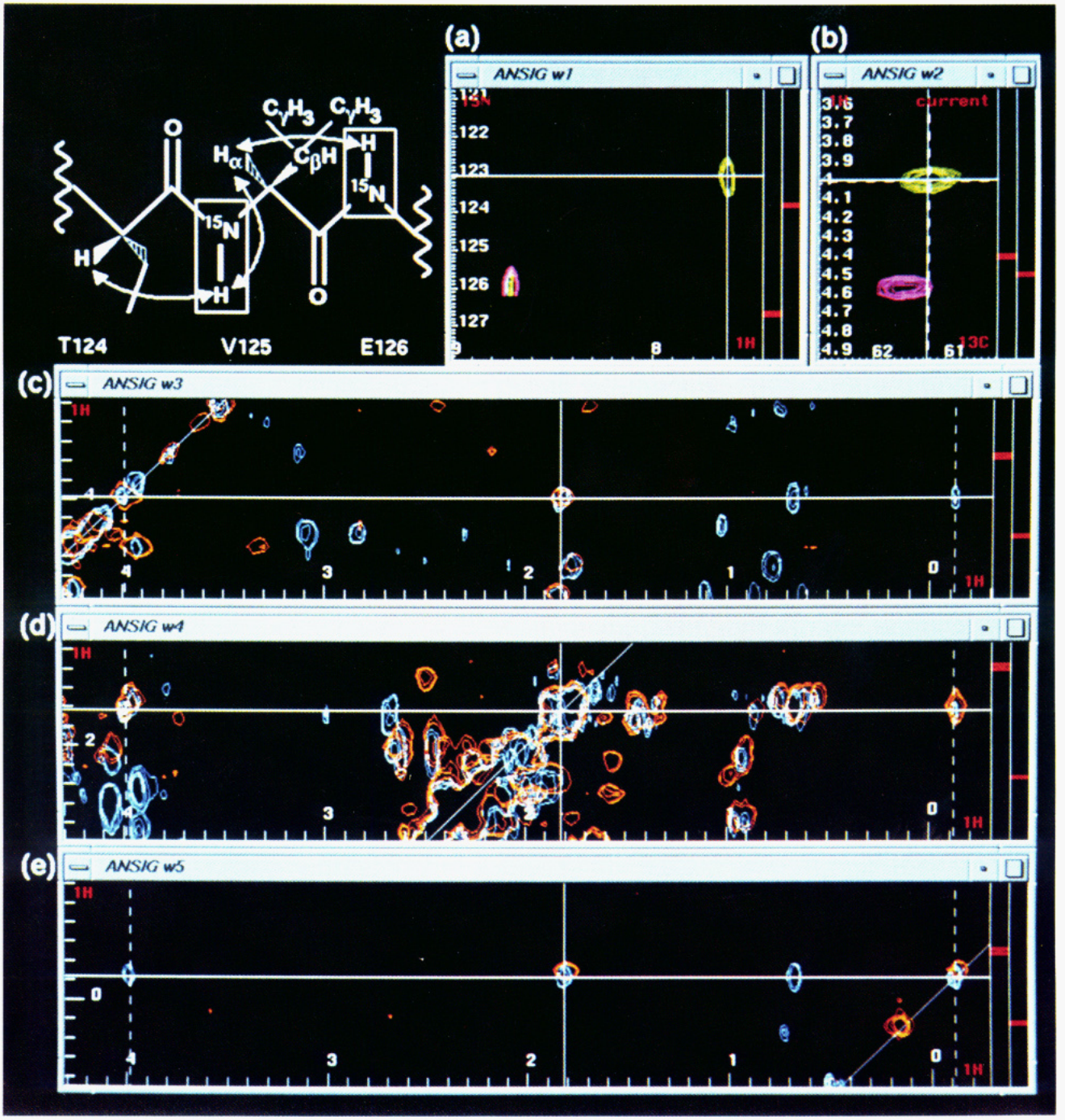

FIGURE 1: Illustration of the assignment strategy for the aliphatic residues (excluding glycine and proline) of ras p21 (1–166)·GDP. Panel a shows the overlaid 2D planes ($f_3 = {}^{15}N$ and $f_4 = {}^{1}H_N$), at the $f_1 = {}^{1}H_\alpha$ and $f_2 = {}^{13}C_\alpha$ chemical shifts of Val-125, from the HCANNH (green) and the HCA(CO)NNH (magenta) spectra. Panel b shows the orthogonal 2D planes ($f_1 = {}^{1}H_\alpha$ and $f_2 = {}^{13}C_\alpha$), at the $f_3 = {}^{15}N$ and $f_4 = {}^{1}H_N$ chemical shifts (also of Val-125) indicated by the cursors in panel a. Panels c–e show a series of overlaid 2D planes ($f_1 = {}^{1}H$ and $f_3 = {}^{1}H$) at the chemical shifts corresponding to the $f_2 = {}^{13}C_\alpha$ (a), $f_2 = {}^{13}C_\beta$ (b), and $f_2 = {}^{13}C\gamma$ (e) chemical shifts of Val-125 from the HCCH-COSY (orange) and HCCH-TOCSY (light blue) spectra. In each case the horizontal cursor marks the corresponding ${}^{1}H_\alpha$, ${}^{1}H_\beta$, and ${}^{1}H_\delta$ chemical shifts. The assignment strategy is discussed in the text.

attached protons and so a through-bond connection cannot be made between the $^{13}C_\beta$ and $^{13}C_\delta$ nuclei. Instead, we used the 2D NOESY and TOCSY spectra (recorded in D_2O) to obtain some assignments and spin system identifications of the aromatic protons. These assignments were then completed using the 4D $^{13}C/^{15}N$-edited and 3D ^{13}C-edited NOESY spectra. Statistically, it is likely that the most intense cross peaks in NOESY spectra result from intraresidue NOE interactions. For larger proteins like ras p21 (18.9 kDa) both the 4D $^{13}C/^{15}N$-edited (Kay *et al.*, 1990) and $^{13}C/^{13}C$-edited (Clore *et al.*, 1991; Zuiderweg *et al.*, 1991) NOESY experiments are not particularly sensitive; because the T_2s in larger proteins are shorter, they are more adversely affected by the extra magnetization-transfer steps in ^{15}N- or ^{13}C-edited NOESY spectra. In addition, 4D experiments are less sensitive than 3D experiments, which are in turn less sensitive than 2D experiments. As a consequence many of the cross peaks in our 4D NOESY spectra resulted from intraresidue interactions. This fact was used to assist in the assignment of the aromatic resonances. When the appropriate 2D $^{1}H-^{13}C$ plane at the $^{1}H_N$ and ^{15}N chemical shifts appropriate for a particular aromatic residue amide was displayed, in several cases a cross

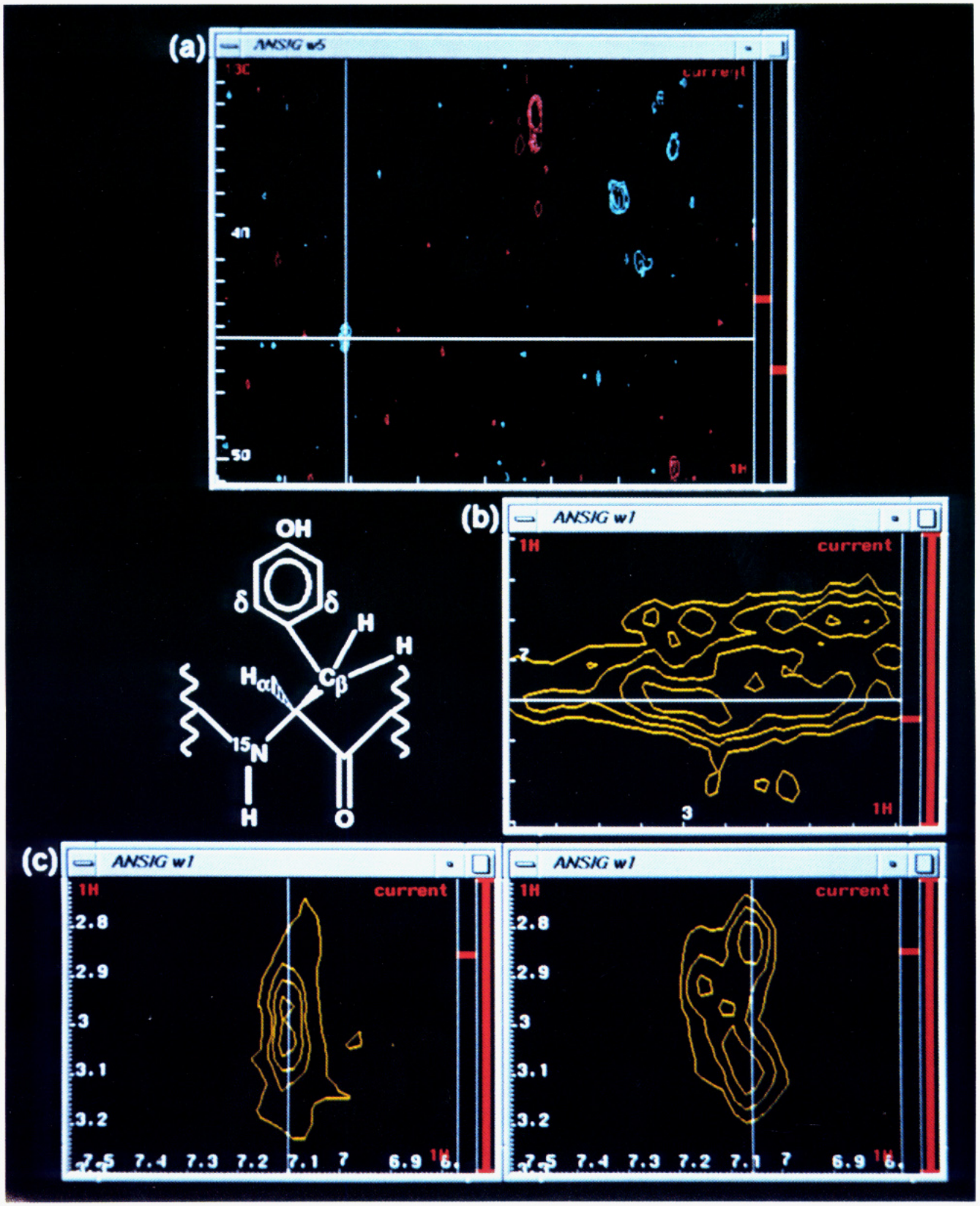

FIGURE 2: Illustration of the assignment strategy for the aromatic residues of ras p21 (1–166)·GDP. Panel a shows a 2D plane (f_1 = ^{1}H and f_2 = ^{13}C), at the f_3 = ^{15}N and f_4 = ^1H_N chemical shifts for Tyr-64, from the 4D ^{13}C/^{15}N-edited NOESY spectrum (aliased cross peaks are light blue, others are magenta). Panel b shows the 2D plane (f_1 = ^{1}H and f_3 = ^{1}H), at the f_2 = $^{13}C_\delta$ chemical shift identified from panel a, from the 3D ^{13}C-edited NOESY spectrum. The cursor marks the corresponding $^1H_\delta$ chemical shift. Panel c shows the symmetry-related cross peaks (f_1 = ^{1}H and f_3 = ^{1}H) at the f_2 = $^{13}C_\beta$ chemical shifts for Tyr-64 (left, $^{13}C_\beta$ = 38.25 ppm) and Tyr-71 (right, $^{13}C_\beta$ = 37.79 ppm) from the same spectrum. The assignment strategy is discussed in the text.

peak in the aromatic region could be observed. This was assumed to be due to the intraresidue NOE to the $^1H_\delta/^{13}C_\delta$ of the same residue (see Figure 2a). These assignments were confirmed by displaying the appropriate 2D ^{1}H–^{1}H plane, again using a macro, from the 3D ^{13}C-edited NOESY spectrum. For example, by marking the $^1H_\delta$, $^{13}C_\delta$ cross peak

in the 4D $^{13}C/^{15}N$-edited NOESY spectrum (note that it is aliased), we can display the appropriate plane from the 3D ^{13}C-edited NOESY spectrum in Figure 2b. In this case the $^1H_\beta$ protons of Tyr-64 overlap with those from Tyr-71, but as mentioned above, if we display the contours of the symmetry-related cross peak, then the two sets of cross peaks can often be resolved if the $^{13}C_\beta$ chemical shifts are different for the two residues (see Figure 2c). We found that the ability to look quickly at a cross peak and its symmetry-related partner was often very useful to resolve ambiguities in this 3D NOESY spectrum (see Analysis of NOESY Spectra, below). Once an unambiguous connection had been made between the backbone or side chain and the aromatic ring $^1H_\delta/^{13}C_\delta$, the rest of the ring could be identified by combined use of the 2D NOESY, 2D TOCSY, and 3D ^{13}C-edited NOESY spectra.

We found that the combination of the 4D $^{13}C/^{15}N$-edited and 3D ^{13}C-edited NOESY spectra was also useful for obtaining some assignments of long side-chain residues like arginine or lysine using a similar approach to that used for the assignment of proline side chains (see below). The difficulty with using this spectrum for assignments is, of course, that they contain cross peaks due to interactions with protons on sequential or occasionally more distant residues. This led us to develop new 4D NMR experiments in which these side-chain (^1H and ^{13}C) resonances are correlated with the backbone (^1H_N and ^{15}N) resonances via through-bond interactions (Richardson *et al.*, 1993; Clowes *et al.*, 1993). These experiments remove the ambiguity inherent in assignments based on NOESY spectra, but at the time of carrying out this assignment these experiments were not available. In addition, they are not so sensitive as the 3D NOESY spectra and may therefore not be applicable to such large proteins as the approach described here.

Assignment of the Glycine Residues. In the pulse sequences used to record the 4D HCANNH and HCA(CO)NNH spectra, one of the delays (τ_1 in Figure 1; Boucher *et al.*, 1992b) was set to optimize the sensitivity of cross peaks from residues with a single α proton. If τ_1 is set to 3.4 ms, cross peaks from glycine residues are not detected. However, one does obtain the ^1H_N and $^{15}H_N$ assignments of glycine residues when the protein is assigned in the amino- to carboxy-terminal direction (Campbell-Burk *et al.*, 1992), so it only remained to assign the $^1H_\alpha$ and $^{13}C_\alpha$ resonances. It would have been a simple matter to record a 3D HCA(N)NH spectrum with τ_1 set to 1.7 ms to optimize detection of cross peaks from glycine residues, but we instead used a combination of the 3D ^{15}N-edited NOESY or TOCSY spectra and the 3D HCCH-COSY spectrum as they had already been recorded. Knowing the ^1H_N and ^{15}N chemical shifts (from the 4D experiment), we can display the appropriate plane of the 3D ^{15}N-edited NOESY or TOCSY spectrum and obtain the $^1H_\alpha$ chemical shifts; the TOCSY spectrum was not used exclusively as the sensitivity of this experiment was rather poor for the ras p21 protein. We can then display the appropriate region of the 2D ^1H–^1H plane from the HCCH-COSY spectrum and load up all the contours in the ^{13}C dimension. The cross peaks for the glycine are readily recognized as the symmetry-related peaks are uniquely found in the same ^{13}C plane because both $^1H_\alpha$ protons are attached to the same ^{13}C nucleus. In addition, the $^{13}C_\alpha$ chemical shift for glycine is very characteristic [see, e.g., Clore *et al.*, (1990)].

Assignment of the Proline and Methionine Residues. The assignment of proline residues also represents a special case with our assignment strategy, because proline residues lack an amide proton and cannot give cross peaks in the 4D HCANNH and HCA(CO)NNH spectra. The assignment of the $^1H_\alpha$ and $^{13}C_\alpha$ resonances of proline residues is possible when the protein is assigned in the carboxy- to amino-terminal direction (Campbell-Burk *et al.*, 1992). We were unable to extend these assignments past the $^1H_\beta$ protons using the 3D HCCH-COSY or TOCSY spectra as typically no further cross peaks were detected; surprisingly, this result was true for TOCSY spectra recorded with both short (7 ms) and longer (24 ms) mixing times and contrasts with the experience of others [see, e.g., Clore *et al.* (1990)]. Instead, we relied on a careful analysis of cross peaks in the 3D ^{13}C-edited NOESY spectrum. The $^1H_\alpha$ and $^{13}C_\alpha$ chemical shifts, obtained from the 4D HCA(CO)NNH spectrum, allowed us to display the appropriate 2D ^1H–^1H plane containing cross peaks resulting from NOE interactions of protons close in space to these nuclei. Because the $^1H_\alpha$ proton is always close in space to the $^1H_\beta$ protons, we expect strong cross peaks to result from this interaction (see Figure 3a). By looking for the symmetry-related cross peaks, we can resolve ambiguities (as demonstrated in Figure 2), where required, and obtain the $^{13}C_\beta$ chemical shift. We can then display that 2D ^1H–^1H plane in which we expect strong cross peaks to the $^1H_\alpha$ and $^1H_\gamma$ protons (Figure 3b) and repeat the whole procedure. Ultimately we can compare all the appropriate 2D ^1H–^1H planes and check for internal consistency, in particular that all the intensities are as expected (see Figure 3). This type of analysis was also required for some of the other long side-chain residues, in particular some lysine and arginine residues. For each of the proline residues (34, 110, and 140) the $^{13}C_\beta$ and $^{13}C_\gamma$ chemical shifts (Shirakawa *et al.*, 1993) and the lack of sequential $^1H_\alpha$–$^1H_\alpha$ NOEs from the preceding residue were all consistent with a trans conformation.

The methionine methyl ^1H and ^{13}C resonances do not have any cross peaks in the HCCH spectra so again their assignment required the 3D ^{13}C-edited NOESY spectrum. By analysis of initial structures computed from the unambiguous NOE data, potential neighbors could be identified. The spectrum was then inspected in order to locate the appropriate cross peaks. This was aided by the knowledge of the expected chemical shifts for the $^1H_\epsilon/^{13}C_\epsilon$ nuclei in methionine. In addition, these resonances are unusually sharp, so the presence of residual truncation artifacts associated with the latter cross peaks often helped confirm their assignment.

Although this analysis is certainly not as unambiguous as an analysis of the 3D HCCH spectra, it does provide an alternative when the sensitivity is inadequate in the spectra resulting from the through-bond experiments. In order to minimize the possibility of ambiguities and our making errors, we left this part of the assignment until the final stages.

Assignment of the GDP Resonances. The GDP used in preparation of the NMR samples was unlabeled, but some tentative assignments were possible and ultimately contributed useful structural data (see below). The H8 ring proton in GDP (6.06 ppm) was readily assigned in the 2D TOCSY and NOESY spectra as it is found in an otherwise empty region of the spectrum. Tentative assignments of the H1′ → H4′ protons in the ribose ring were also made from the 2D TOCSY spectrum, and assignments of the exchangeable protons were possible from 1D spectra recorded using a (1:1) pulse for water suppression.

Analysis of Breaks in the Assignment Using Our 4D NMR Strategy. In the previous assignment of the backbone resonances using our 4D NMR strategy (Campbell-Burk *et al.*, 1992), apart from the expected missing assignments of the glycine and proline residues, we failed to obtain the

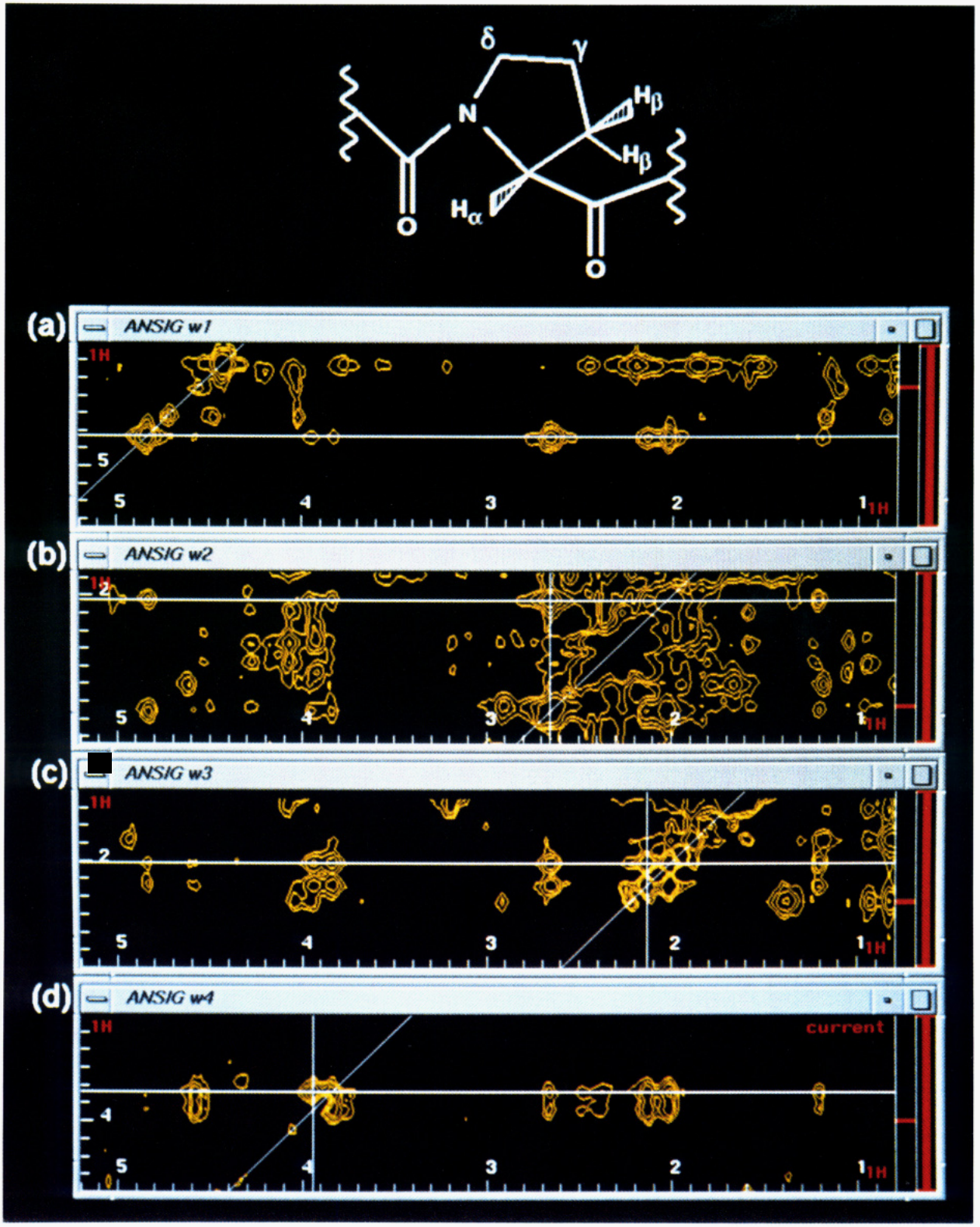

FIGURE 3: Illustration of the assignment strategy for the proline and some long side-chain residues of ras p21 (1–166)·GDP. The figure shows a series of 2D planes (f_1 = ^{1}H and f_3 = ^{1}H), at the chemical shifts corresponding to the f_2 = ^{13}Cα (a), f_2 = ^{13}C$_\beta$ (b), f_2 = ^{13}C$_\gamma$ (c), and f_2 = ^{13}C$_\delta$ (d) chemical shifts of Pro-34, from the 3D ^{13}C-edited NOESY spectrum. In each case the horizontal cursor marks the corresponding ^{1}H$_\alpha$, ^{1}H$_\beta$, ^{1}H$_\gamma$, and ^{1}H$_\delta$ chemical shifts. The assignment strategy is discussed in the text.

complete assignments for Asn-86, Thr-87, Ser-127, and Thr-158. The amide proton of Thr-87 proved not to be visible in any of the spectra at the pH we used (6.5) although it has been reported at pH 5.5 (Muto *et al.*, 1993). We suspect that strong ^{13}C$_\alpha$–^{13}C$_\beta$ coupling may have prevented the HCANNH and HCA(CO)NNH experiments working effectively for Ser-127 (^{13}C$_\alpha$, 62.6 ppm; ^{13}C$_\beta$, 62.2 ppm) and Thr-158 (^{13}C$_\alpha$, 67.3 ppm; ^{13}C$_\beta$, 67.7 ppm). The lack of assignments for Asn-86 can now be attributed to severe overlap (^{1}H$_\alpha$ and ^{13}C$_\alpha$) with Asn-85. However, we were able to resolve this problem in the later stages of the assignments using the 3D HCCH spectra, because the two residues had different ^{13}C$_\beta$ chemical shifts.

Analysis of the NOESY Spectra. The 3D ^{13}C-edited and ^{15}N-edited NOESY spectra proved to be the most useful for

obtaining the necessary interresidue restraints for the structure determination. The analysis of the 3D NOESY spectra was greatly facilitated by the use of macros in ANSIG which display strips from the appropriate 2D planes containing cross peaks from the $^1H_N/^{15}N$ (^{15}N-edited spectrum), $^1H_\alpha/^{13}C_\alpha$, $^1H_\beta/^{13}C_\beta$, etc. nuclei (^{13}C-edited spectrum) for a given residue. Long-range NOESY cross peaks were assigned by reference to the list of possible assignments output by ANSIG; the ability to quickly display the symmetry-related regions in the ^{13}C-edited spectrum was essential to resolve ambiguities. It was possible in a large majority of cases to find unambiguously the symmetry-related partner of a cross peak, thus giving the ^{13}C chemical shift of each of the carbons covalently attached to the two protons involved.

As mentioned above, for ras p21 (1–166)·GDP (18.9 kDa), the 4D $^{13}C/^{15}N$-edited and $^{13}C/^{13}C$-edited NOESY experiments were not particularly sensitive, and during the assignment it became clear that neither 4D spectrum would give enough structurally interesting information. We therefore concentrated our efforts on assigning the 3D ^{15}N-edited and ^{13}C-edited spectra completely, occasionally using the 4D NOESY spectra to resolve ambiguities or to verify assignments.

In order to complete the assignment of long-range cross peaks in the 3D NOESY spectra, we used a set of initial structures computed from distance restraints (see below) derived from only the completely unambiguous NOEs. The ANSIG program can give information on which particular combinations of potential assignments for a NOESY cross peak are plausible, based on the interproton distances observed in a set of initial structures, and using this facility we were then able to go on and assign practically all the cross peaks in the two 3D NOESY spectra.

NOE-Derived Distance Restraints. The assigned NOESY cross peaks were volume-integrated by simple summing of the values of the spectrum matrix data points within a box around the cross-peak center; the values for cross peaks involving methyl resonances were divided by 3. The intensity value for each NOE was taken as the average of the corresponding cross peaks in every 2D, 3D, or 4D spectrum where that NOE appeared, and had been assigned, including symmetry-related cross peaks. No further attempt was made to correct for the differences in magnetization transfer in the 3D NOESY experiments due to effects of different couplings or relaxation rates of the different ^{13}C or ^{15}N nuclei. The NOE intensities were converted into four distance restraint classes where the lower bounds were all set to 0.0 Å (rather than 1.8 Å, the sum of the van der Waals radii) in order to improve the performance of the simulated annealing protocol (Hommel *et al.*, 1992): strong (0.0–2.7 Å), medium (0.0–3.3 Å), weak (0.0–5.0 Å), and very weak (0.0–6.0 Å). The latter intensity class was introduced as a means to partially account for spin diffusion. The NOE intensities were calibrated by reference to known distances in well-defined sections of secondary structure. Center averaging of degenerate or nonstereospecifically assigned protons (equivalent to the pseudoatom approximation) was used in the structure calculations, necessitating the addition of appropriate distance corrections to the upper distance bounds (Wüthrich *et al.*, 1983). The first list of NOE-derived constraints, based purely on unambiguously assigned cross peaks, contained a total of 2736 distance restraints, of which 578 were long range (i to $i \geq 5$). An iterative procedure was employed to obtain a more complete set of restraints by using structures computed from these initial restraints to resolve remaining ambiguities. The final list of NOE-derived distance constraints contained a total of 3167 distance restraints, of which 1081 were intraresidue, 619 sequential, 478 short range (i to $i < 5$), and 989 long range (i to $i \geq 5$).

Other Restraints Used in the Structure Calculations. We obtained 14 ϕ restraints from an analysis of the intensity of the ^1H_N–$^1H_\alpha$ cross peaks, compared to the diagonal peaks, in the 3D ^{15}N-edited TOCSY spectrum (Archer *et al.*, 1993) and 54 χ_1 restraints from an analysis of the $^3J_{H\alpha H\beta}$ and $^3J_{C'H\beta}$ couplings in the SOFT HCCH-E.COSY and HCCH-COSY spectra (Eggenberger *et al.*, 1992). The methyl groups of a total of 10 (out of 15) valine reidues could be stereospecifically assigned on the basis of the χ_1 dihedral angle derived from the $^3J_{H\alpha H\beta}$ coupling constant and the intraresidue NOEs (Zuiderweg *et al.*, 1985; but note that the convention for labeling valine methyls was accidently reversed in their paper).

Although we also obtained many stereospecific assignments of the $^1H_\beta$ methylene protons, these were still treated as pseudoatoms in the structure calculations. We found that the relative intensities of the two $^1H_\alpha$–$^1H_\beta$ NOESY cross peaks for many residues were nearly equal in intensity, regardless of the χ_1 dihedral angle. This indicates that spin diffusion affects the methylene proton NOEs significantly, which is to be expected with NOESY mixing times of 100 ms in a protein of this size (18.9 kDa). We suggest that in these circumstances distance restraints involving methylene protons should be referred to the pseudoatom positions (Wüthrich *et al.*, 1983).

Signals for several side-chain hydroxyl protons were detected in the 3D ^{15}N-edited NOESY spectrum and could be assigned from inspection of the initial structures. A total of 54 hydrogen bonds were identified on the basis of slowly exchanging amide protons and the side-chain hydroxyl proton of Ser-145, where the acceptor nucleus was unambiguous from inspection of the initial structures. For each ^1H_N hydrogen bond, two distance restraints were included, one for the amide proton to acceptor distance (1.8–2.4 Å) and one for the amide nitrogen to acceptor distance (2.6–3.4 Å), giving a total of 109 distance restraints.

As well as determining eight ligand to protein NOEs, several further restraints were added in the final stages to help locate both the magnesium ion and the GDP molecule, and they require special justification. First, Tucker *et al.* (1986) have shown that the β-phosphate of the GDP molecule interacts with the magnesium ion, and electron paramagnetic resonance (EPR) studies have suggested that the magnesium ion is coordinated to four water molecules (Latwesen *et al.*, 1992). In addition, it is known that mutation of Ser-17 to alanine prevents magnesium binding (Farnsworth & Feig, 1991). On the basis of these studies we included appropriate restraints to the magnesium ion. We found five slowly exchanging amide protons (Gly-15, Ser-17, Ala-18, Ala-146, and Lys-147) where there was no possible acceptor nucleus other than the β- (15 and 17) and α-phosphates (18) or the carbonyl oxygen (146 and 147) of the GDP molecule. Two other amide protons (Gly-13 and Lys-16) were also constrained to be near the β-phosphate on the basis of their unusual low-field ^1H chemical shifts (10.58 and 10.59 ppm, respectively) (Redfield & Papastavros, 1990, and references therein). Finally, the ring N-1 and the exocyclic 2-amino group of the GDP were constrained to be hydrogen bonded to Asp-119 on the basis of mutational evidence (Sigal *et al.*, 1986; Hwang & Miller, 1987). Sigal *et al.* (1986) showed that mutation of Asp-119 to Ala reduced the affinity of binding of both GDP and GTP (20-fold) as well as the specificity of binding of GDP over inosine diphosphate. Hwang and Miller (1987) took advantage of the known structure of the ET-Tu·GDP complex to

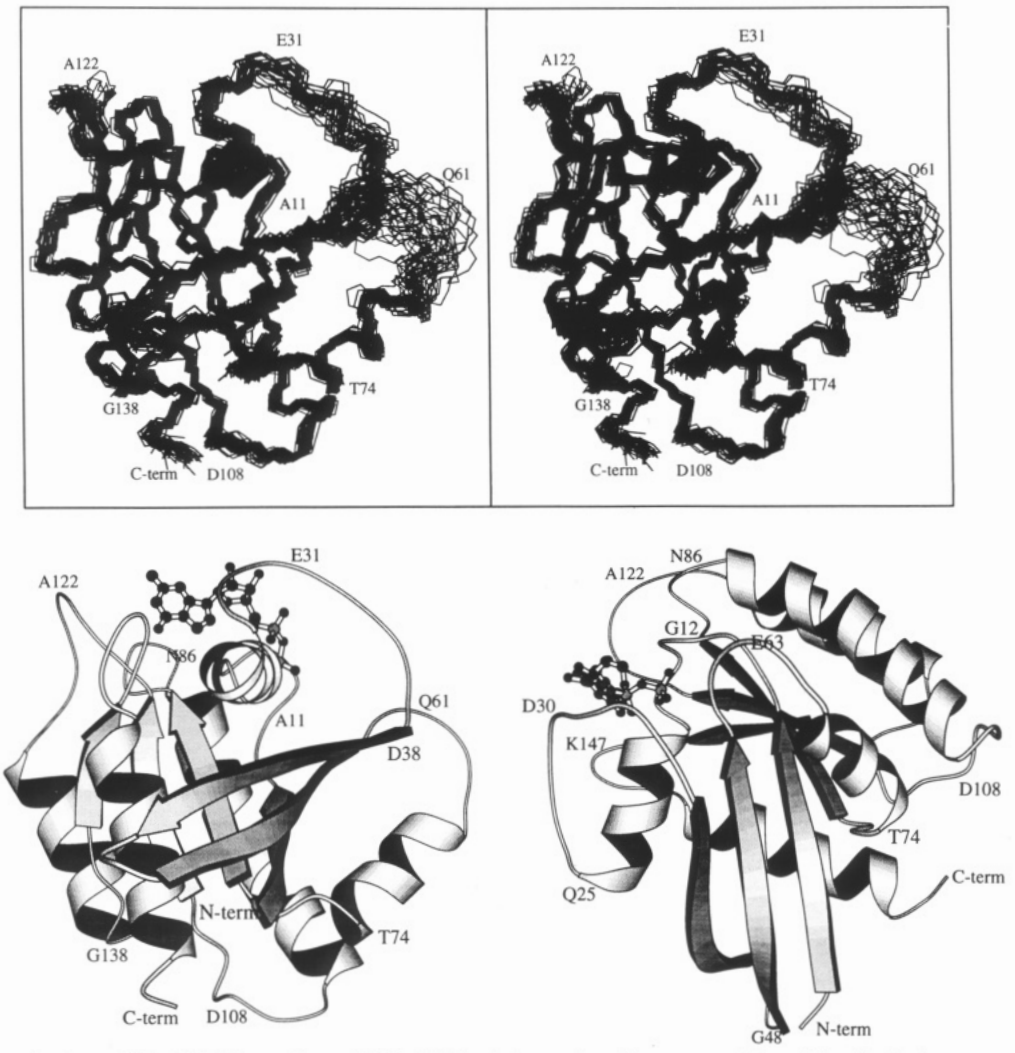

FIGURE 4: Solution structure of the GDP form of ras p21 (1–166). A stereoview of a superposition of the 40 final structures, showing the backbone, after a least squares fit is shown in panel a (top). In panels b and c (bottom left and right, respectively), two different schematic representations of the structure are shown; panel b corresponds to the same orientation as that in panel a. These drawings and those in Figures 6 and 8 were generated using Molscript (Kraulis, 1991).

change the nucleotide specificity of EF-Tu from GDP to xanthosine 5′-diphosphate by mutating Asp-138 (equivalent to Asp-119 in ras p21) to asparagine. This result strongly suggested that Asp-138 interacts with GDP via the types of hydrogen-bonding interaction discussed above [see also Lancelot *et al.* (1979)].

Structure Calculations. The initial structures were computed solely from the distance restraints derived from those NOEs that could be assigned unambiguously. These computations used the program X-PLOR (Brünger, 1992) and started from an extended strand (Nilges et al., 1988). They resulted in structures that had a root mean square (rms) deviation, for the C_α atoms in the well-defined part of the molecule (see below), of about 1.5 Å. These structures displayed a unique fold and could be used to determine a majority of the hydrogen bond acceptors and to resolve numerous ambiguous NOEs. Since the fold was uniquely determined already in the initial structures, a shortened protocol starting from these structures was used in the later iterations in order to reduce the computing time. In the absence of methods to deal adequately with the differences in magnetization transfer in the 3D NOESY experiments due to effects of different couplings or relaxation rates of the different ^{13}C or ^{15}N nuclei, no attempt to use relaxation matrix refinement procedures was attempted.

3D Solution Structure. A total of 40 final structures (see Figure 4) were calculated from the experimental restraints (see Table 1 for the structural statistics). The structures are well-defined, with a rms deviation about the average structure of 0.78 Å for the backbone atoms and 1.29 Å for all heavy atoms (see Table 2). However, the superposition of the computed structures (see Figure 4a) and a plot of the rms deviation of the C_α atoms from the average structure (see Figure 5a) show that two regions in particular are not well-defined; they comprise residues 30–38 and residues 58–66 the second and fourth loops (L2 and L4), respectively. If these regions are excluded from the analysis, the corresponding rms values are reduced to 0.55 and 1.00 Å, respectively (see Table 2). The positions of the side chains in the protein are in many cases well determined, and two regions showing part of one of the β-sheets in the core (a) and the following α-helix on the surface (b) are shown in Figure 6. This is also evident from a plot of the χ_1 dihedral angle order parameters (Hyberts *et al.*, 1992) against the sequence shown in Figure 5b. In particular, the region around Phe-82 is in a very rigid part of the structure. The resonances of the aromatic protons of Phe-82 are broad, indicative of their being on the edge of slow rotation on the NMR time scale. In addition, many of the exchangeable protons in this region of the protein are slowly exchanging. This region also has very low *B*-factors in the

Table 1: Structural Statistics

structural statistic[a]	⟨SA⟩	$SA_{av\text{-}rmin}$
rms deviation from the experimental distance (Å) and dihedral angle (deg) restraints[b]		
distance restraints (3300)	0.026	0.023
dihedral angle restraints (69)	0.67	0.67
no. of violations of the experimental restraints[c]		
distance restraints (>0.5 Å)	0.72	1
dihedral angle restraints (>4°)	0.45	1
$E_{L\text{-}J}$[d] (kcal/mol)	−410 ± 66	−625
rms deviations from ideal covalent geometry		
bonds (Å)	0.0039	0.0036
angles (deg)	0.62	0.58
impropers (deg)	0.42	0.36

[a] The notation is as follows: ⟨SA⟩ is the average value for the final 40 simulated annealing (SA) structures; $SA_{av\text{-}rmin}$ is the value for the mean structure obtained by averaging the coordinates of the individual SA structures best fitted to each other and minimizing the energy with all restraints. [b] The number of restraints is given in parentheses. [c] The maximum number of violations in an individual SA structure is 2 and nearly always involves restraints for Val-109 (see text). [d] $E_{L\text{-}J}$ is the Lennard-Jones van der Waals energy calculated with the CHARMM (Brooks *et al.*, 1983) force field (not included in the structure calculations).

Table 2: Atomic rms Differences[a]

	residues	backbone atoms (Å)	non-hydrogen atoms (Å)
⟨SA⟩ vs SA_{av}	1–166	0.78	1.29
	1–29, 39–57, 69–166	0.55	1.00
SA_{av} vs $SA_{av\text{-}rmin}$	1–166	0.37	0.67
SA_{av} vs X-ray·GDP[b]	1–166	1.29	1.93
	1–29, 39–57, 69–166	0.99	1.66
SA_{av} vs X-ray·GPPNP[c]	1–166	1.48	2.31
	1–29, 39–57, 69–166	0.90	1.54

[a] The notation is as in Table 1, with the addition that SA_{av} is the mean structure obtained by averaging the coordinates of the individual SA structures best fitted to each other without energy minimization. [b] X-ray·GDP refers to the structure of the complex of ras p21 (1–189) with GDP determined at 2.0-Å resolution (PDB code 4Q21; Prive *et al.*, 1992). [c] X-ray·GPPNP refers to the structure of the complex of ras p21 (1–166) with GPPNP determined at 1.35-Å resolution (PDB code 5P21; Pai *et al.*, 1990).

X-ray structures. The stereochemistry of the structures, as judged by the ϕ and ψ angles in a Ramachandran plot, is good (data not shown).

A schematic view of the solution structure of ras p21·GDP (1–166) is shown in Figure 4. The fold can be described as an α/β structure with a β-sheet consisting of one antiparallel and five parallel strands. The β-sheet curls around the C-terminal helix with the first helix lying at nearly right angles to it. On its convex side, the β-sheet is flanked by three more helices. The GDP binding site is located at the carboxy edge of the β-sheet, similar to other nucleotide-binding open β-sheet structures. The binding site is formed by several loops as well as the N-terminal end of the first helix. The topology of the fold is identical to that found in the X-ray diffraction studies (Pai *et al.*, 1989; Tong *et al.*, 1989). The secondary structure elements are also the same as those found in the crystal structure of ras p21·GDP (1–171) (Tong *et al.*, 1991), except that, in the solution structure, helix-2 starts at residue 65 or 66 (instead of at residue 69 in the crystal structure). In addition, in the solution structure the C-terminal helix ends at residue 166, because the fragment we used in our work was shorter than that used for the crystal structure. In both the solution and crystal structures helix-3 is kinked around residue 93.

The poorly defined regions in the structure could have been due either to a lack of structural restraints or to genuine mobility. The latter was suggested by strong ^1H_N–$^1H_\beta$ cross peaks for residues 61–64 in the ^{15}N-edited TOCSY spectrum, but to more rigorously assess this, we studied the backbone dynamics of the protein by measuring the heteronuclear NOEs and T_1s and T_2s in the ^{15}N-labeled protein (Kay *et al.*, 1989). Plots of the heteronuclear NOEs, T_1s, T_2s, and T_1/T_2s against the amino acid sequence are shown in Figure 7. They clearly show that the regions comprising residues 27–32, 58–66, and 107–109 have significant rapid internal motions on the nanosecond time scale. The region 107–109 is relatively well-defined in the NMR structures (but, see below). However, the first two regions correlate well with the regions that are poorly defined by the NMR data (see Figures 4a and 5a). As in part predicted from the X-ray crystallographic studies and molecular dynamics simulations (Foley *et al.*, 1992), this strongly suggests that they are ill-defined due to genuine mobility, not because of a lack of experimental restraints. The remaining violations of the experimental restraints in the simulated annealing structures involve almost exclusively residue Val-109. The restraints that are violated most often are the Val-109 $H_{\gamma 2}$ to Met-111 H_α distance and the χ_1 dihedral angle restraint of Val-109. Both these restraints are derived from clear and unambiguous NOE and J coupling constant data. The high ^{15}N T_2 and low heteronuclear NOE values for Val-109 and the residues immediately preceding it suggest that residues 107–109 (and possibly Pro-110, since its ^{15}N relaxation parameters cannot be measured) can exist in more than one conformation and that these conformations are in fast exchange with each other. These conformations may give rise to NOEs which cannot be satisfied by a single structure.

Comparison with the X-ray Structures. The solution structures were carefully examined for differences from the published structures determined by X-ray crystallography. A comparison of the computed NMR structures with the most highly refined X-ray structure of the GDP form of the ras p21 (1–189) protein (Milburn *et al.*, 1990; Prive *et al.*, 1992) showed, not surprisingly, significant differences in the two loops (L2 and L4) found to be mobile by NMR spectroscopy (see above). However, the NMR structures also show a consistent difference in the orientation of helix-2 (residues 66–75); this difference (see Figure 8a) is also seen in the crystal structure of the GDP form of the ras p21 (1–171) protein (Tong *et al.*, 1989), although in that structure the orientation is slightly closer to the NMR structures (data not shown). The average heteronuclear NOEs, T_1s, and T_2s in this region of the protein suggest that the NMR structures are genuinely well-defined between residues 66 and 75. However, it should be noted that Tyr-71 is located in a very similar position in both the NMR and X-ray structures. Furthermore, the GDP molecule and magnesium ion are also located at very similar positions (see Figure 8b). In the X-ray structures of the GDP form of ras p21 (1–166), arising from hydrolysis in the crystal from ras p21·GTP, the interaction between the carboxylate of Asp-57 and the magnesium ion appears to be direct (Schlichting *et al.*, 1990), while in the ras p21 (1–189)·GDP form and several GTP–analogue complexes (Milburn *et al.*, 1990; Pai *et al.*, 1989) the interaction is indirect via an intervening water molecule. The distance between the closest oxygen in the carboxylate of Asp-57 and the magnesium ion in the solution structures is 4.3 ± 0.9 Å, consistent with an indirect interaction.

Implications of the Solution Structure for the Catalytic Mechanism and Interactions with Other Molecules. Extensive genetic and biochemical studies have pinpointed the regions

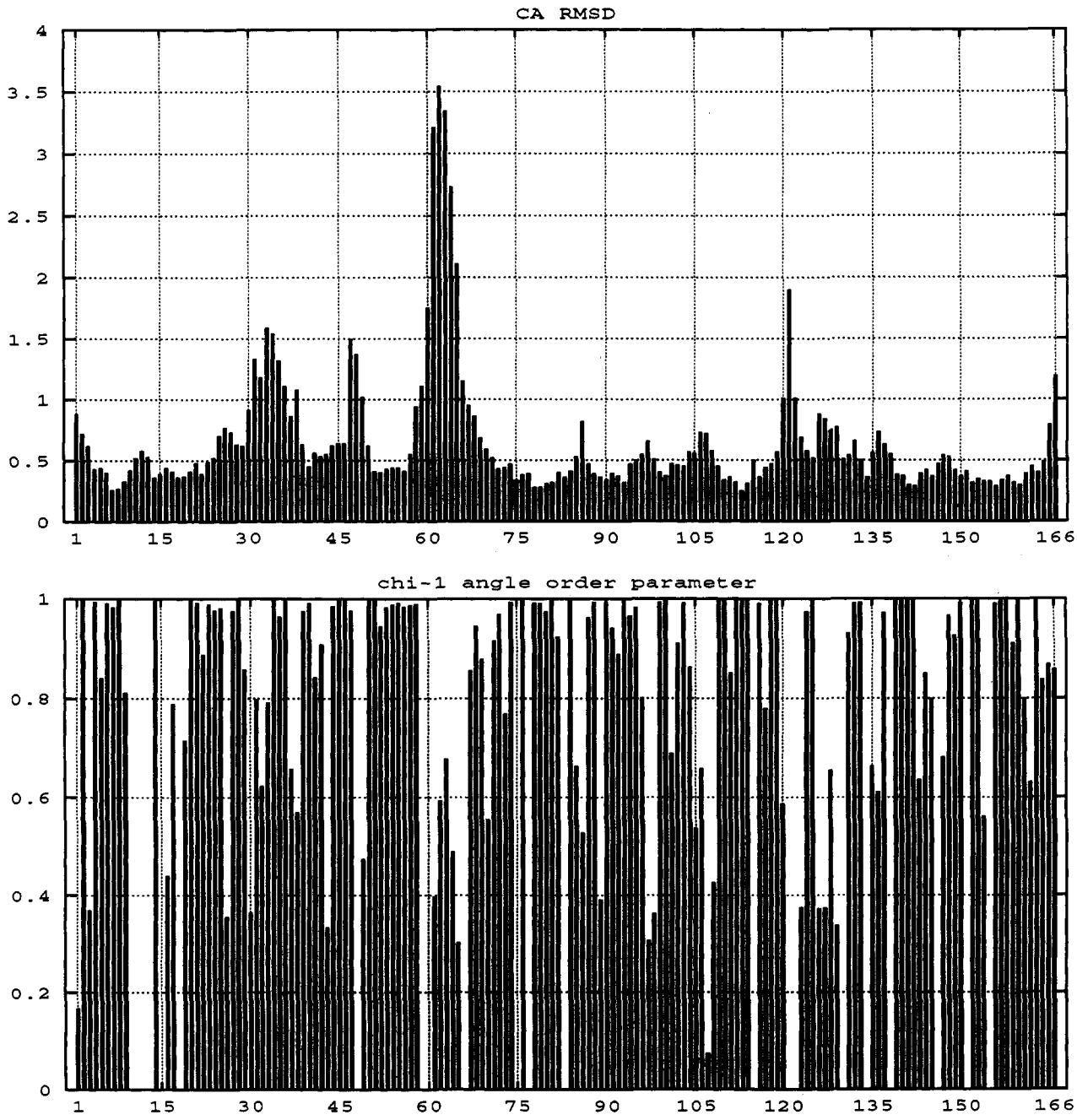

FIGURE 5: Plots of (a, top) the root mean square deviation of the C_α atoms from the average structure and (b, bottom) the χ_1 dihedral angle order parameter (where 0 is totally random and 1 is completely defined) against the amino acid sequence.

of the ras protein involved in interactions with the downstream effectors of ras. Comparison of sequences, deletion of small regions of the protein, "domain swap" experiments with ras-related proteins, and site-directed mutagenesis studies have identified the main region of effector function between residues 26 and 48. Although mutation of residues within this region also affects interactions with GAPs, residues 59–65 are required for GTPase activation but not for ras-induced transformation except in as much as they affect the rate of GTP hydrolysis [for a recent review, see Marshall (1993)]. Mutational analysis implicates residues involved in the coordination of Mg^{2+}·GDP, and the binding of the GDP ring (Mistou *et al.*, 1992), as well as residues 73–75 (Verrotti *et al.*, 1992) and 102–103 (Willumsen *et al.*, 1991). Recently, it has been found that mutations in helix-2 also affect guanidine exchange factor interactions (Howe & Marshall, 1993). Comparison of the three-dimensional structures of the inactive GDP and activated GTP forms of the ras protein determined by X-ray methods reveals significant conformational changes in two regions [for reviews, see Goody *et al.* (1992) and Milburn *et al.* (1990)]: the first comprises residues 32–38 (loop 2) while the second includes loop 4 and helix-2 (residues 60–75). In several of the X-ray studies the electron density for these regions was weak or badly defined, making structural interpretation difficult. Our NMR studies suggest that the regions comprising residues 58–66, and to a lesser extent residues 27–32, are indeed flexible in solution. Moreover, the position of the second helix (residues 66–75) is shown to be different in the solution and crystal structures (Tong *et al.*, 1989; Milburn *et al.*, 1990). These results suggest that NMR spectroscopy may have some advantages for structural studies of proteins that switch between different, energetically finely balanced conformational states, where crystal packing forces are more likely to be able to influence the structure.

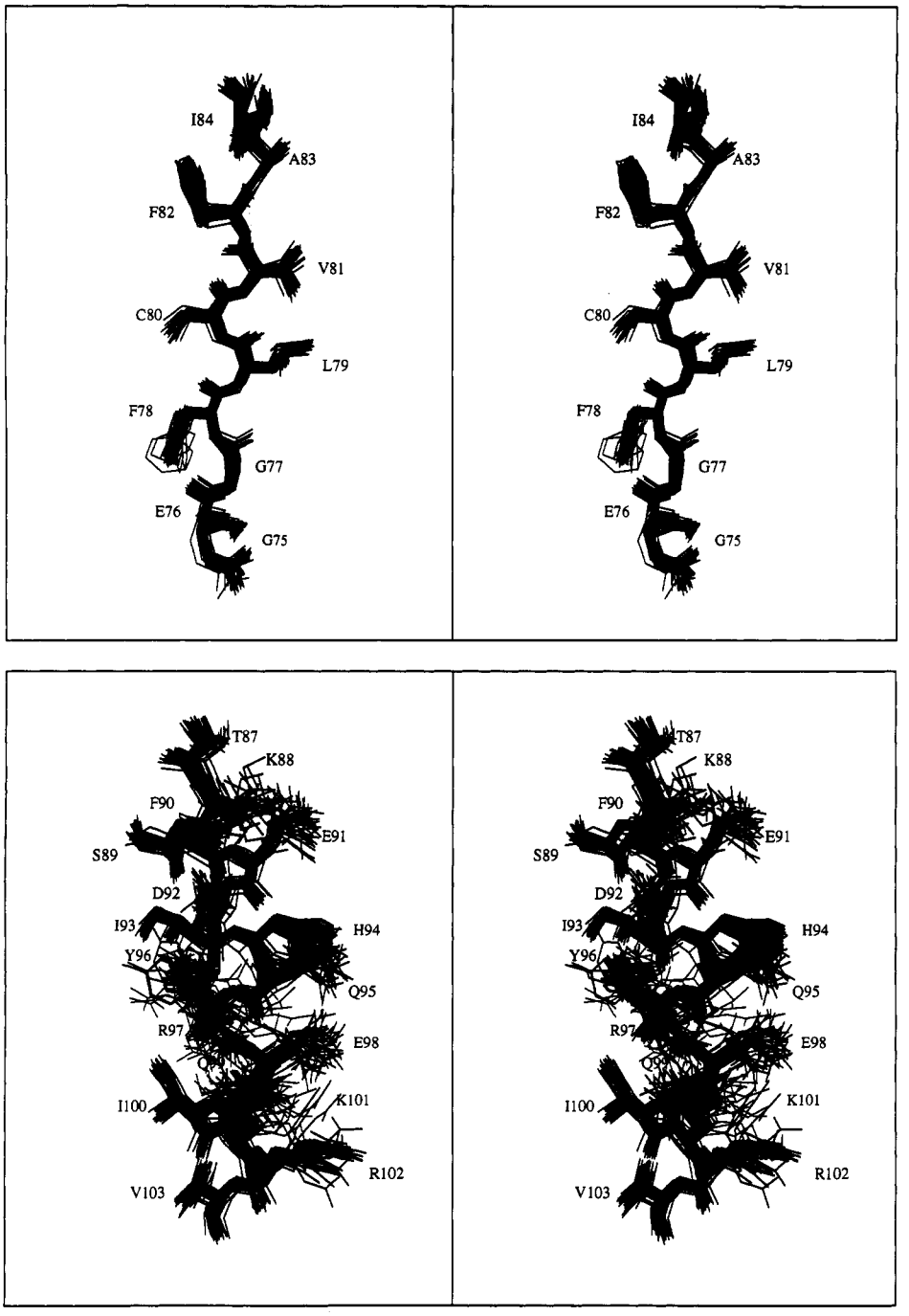

FIGURE 6: Superposition of some of the side-chain residues in two illustrative regions of the protein. In panel a (top) a stereoview of part of one of the β-strands in the core and in panel b (bottom) the following α-helix on the surface of the protein are shown.

The crystallographic work of Kim and co-workers (Milburn *et al.*, 1990) indicated a change in the orientation of helix-2 following exchange of GDP for GDPCP. However, comparison of the GDP and GPPNP forms of ras p21 (1–166) did not reveal any such change (Goody *et al.*, 1992). The direction of helix-2 in our solution structure is closer to the GDP form of ras p21 (1–189) (Milburn *et al.*, 1990; Prive *et al.*, 1992) and ras p21 (1–171) (Tong *et al.*, 1991) than it is to either the GPPNP form (Pai *et al.*, 1990) or the GDPCP form (Milburn *et al.*, 1990; Prive *et al.*, 1992), although it is significantly different from either of them (see Figure 8a). Our results are consistent with the idea that the orientation of helix-2 does change when GDP is exchanged by GTP. However, in the absence of a solution structure for the GTP form of ras p21, the magnitude of this difference remains uncertain. On the basis of model building studies using the GDP form of EF-Tu, Stouten *et al.* (1993) suggested that much larger rearrangements of this region occur upon hydrolysis of GTP to GDP, involving the formation of a helix at residues 63–66 and unraveling of the helix at residues 71–74. Our solution structure of the GDP form of ras p21 does not confirm these predictions. Nevertheless, our finding that there are differences between the solution and at least some of the crystal structures of the GDP form of the protein could be important in understanding the interactions with exchange factors, given that helix-2 is strongly implicated here (Howe & Marshall, 1993).

The flexibility of the region comprising residues 59–65 also has interesting implications for the activation of the intrinsic GTPase activity by GAP proteins. It is possible that none of the conformations modeled in the X-ray structures are, in fact, relevant to the catalytically competent state and that

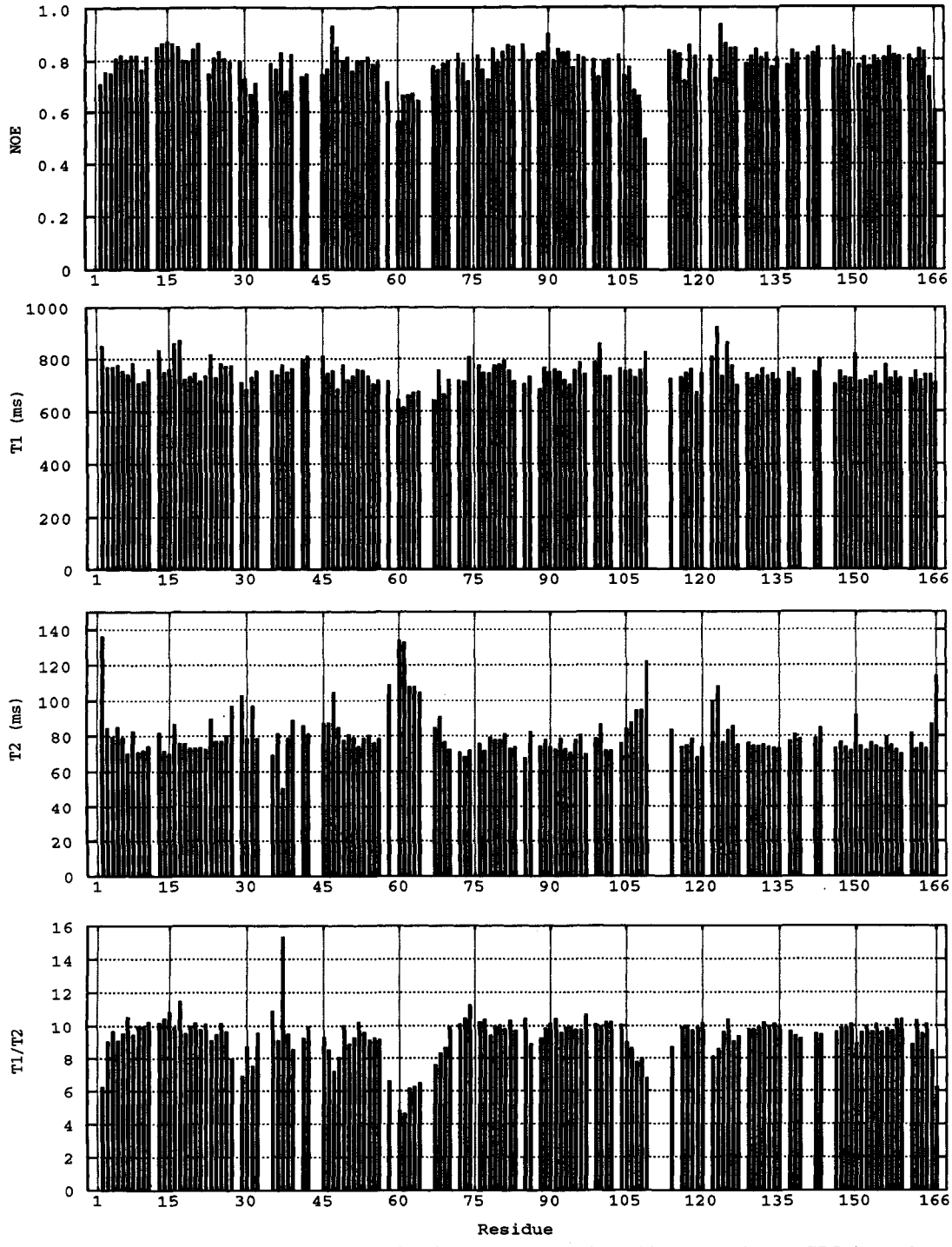

FIGURE 7: Plots of the heteronuclear NOE, ^{15}N T_1, T_2, and T_1/T_2 against the amino acid sequence for the GDP form of ras p21 (1–166).

useful information will only emerge from structural studies of complexes with GAPs. The mobility of loop L4 suggests that GAP proteins may work by freezing out the catalytically active conformation (Pai *et al.*, 1990). In this scenario, the intrinsic catalytic activity would result from the small proportion of time this region of the protein spends in the active conformation. Mutations at position 61 in ras p21, from Gln to most other residues, display reduced intrinsic GTPase activity as well as insensitivity to GAPs (Der *et al.*, 1986b). It is possible that, in the catalytically competent state, the side chain of Gln-61 makes specific interactions that are not possible with other residues. However, if the above hypothesis is correct, another possibility is that mutations of Gln-61 may instead influence the mobility of this region of the protein, thereby affecting the ability of loop L4 to take up its catalytically active conformation (Krengel *et al.*, 1990). Further NMR studies of some of the mutants, in which GTPase activity and/or GAP binding are altered, might well be revealing here. For the protein to activate downstream pathways, it must be able to exist as a transiently stable active GTP form. The mobility of loop L4 may be nature's way of achieving this. Only when GAP binds does the catalytically active conformation become stabilized, leading to a rapid switching off of the signal. In the absence of GAP, hydrolysis of GTP is much slower and the active state is maintained much longer. The hypothesis, of course, assumes that similar mobility will be seen in the GTP form of the protein, and although the available evidence supports this, it does remain to be proven.

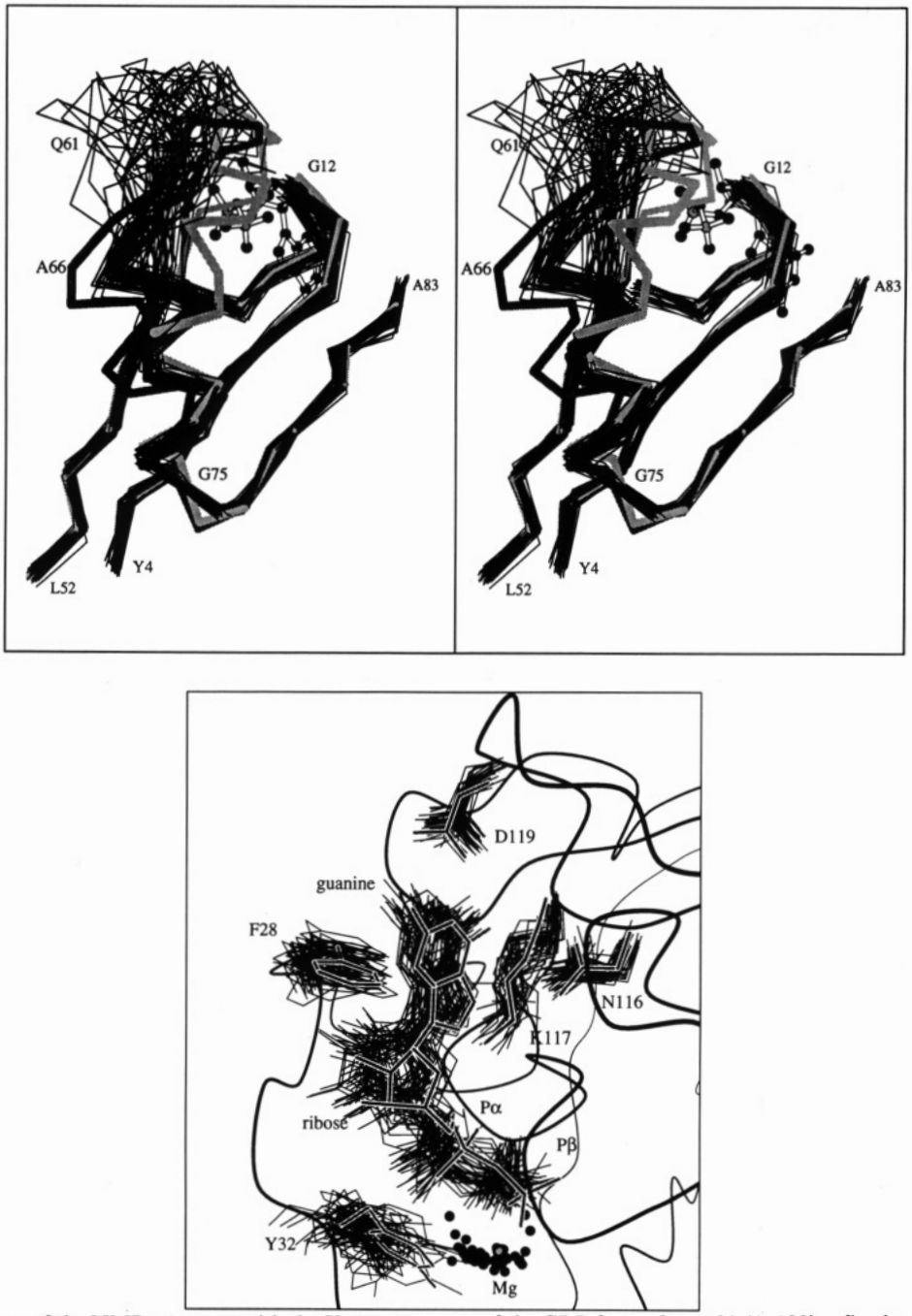

FIGURE 8: Comparison of the NMR structure with the X-ray structures of the GDP form of ras p21 (1–189) refined to 2.0-Å resolution (R value 0.195) (Milburn *et al.*, 1990; Prive *et al.*, 1992) and the GPPNP form refined to 1.35-Å resolution (R value 0.198) (Pai *et al.*, 1989, 1990). Panel a (top) shows a comparison of the different orientations of helix-2 in the family of NMR structures (black), the X-ray structure of the GDP form (gray), and the X-ray structure of the GPPNP form (white); the position of helix-2 in the X-ray structure of ras p21 (1–189)·GDP can be seen to lie outside the envelope of the NMR structures. Panel b (bottom) shows a comparison of the location of the GDP molecule and the magnesium ion, respectively, in the NMR structures (black) and the X-ray structure of the GDP form (gray).

Finally, it has recently been proposed again that the phosphate binding loop 1 (residues 10–18) might adopt two or more conformations in solution (Chung *et al.*, 1993). In agreement with the crystallographic studies (Tong *et al.*, 1989; Milburn *et al.*, 1990), the solution structure of the GDP form of the protein suggests, however, that the structure is well-defined in this region with no evidence from the studies of heteronuclear NOEs, T_1s, and T_2s that there is any conformational flexibility in this region. We feel it is more likely that, as suggested by Krengel *et al.* (1990), the main effect of mutations, e.g., Gly-12 to Val, is to push Gly-60 away from the γ-phosphate where Chung *et al.* (1993) have elegantly demonstrated the backbone amide proton makes crucial interactions in catalysis, perhaps by stabilizing the transition state (Prive *et al.*, 1992).

ACKNOWLEDGMENT

We thank Professors C. Der and A. Wittinghofer for the expression plasmids, Richard DeLoskey, James Krywko, and Richard Yates for expert technical assistance, Bill Broadhurst and Wayne Boucher for computer software, help, and advice, Lewis Kay for help in setting up triple resonance experiments in our laboratories, and Christopher Marshall for a preprint of his paper (Howe & Marshall, 1993). E.D.L. thanks the Royal Society and St. John's College, Cambridge, for a travel grant.

SUPPLEMENTARY MATERIAL AVAILABLE

A virtually complete list of assignments (^{13}C, ^{15}N, and ^{1}H) for ras p21 (1–166) in complex with GDP and Mg (5 pages). Ordering information is given on any current masthead page.

REFERENCES

Archer, S. J., Bax, A., Roberts, A. B., Sporn, M. B., Ogawa, Y., Piez, K. A., Weatherbee, J. A., Tsang, M. L.-S., Lucas, R., Zheng, B.-L., Wenker, J., & Torchia, D. A. (1993) *Biochemistry 32*, 1164–1171.

Ballester, R., Marchuk, D., Boguski, M., Saulino, A., Letcher, R., Wigler, M., & Collins, F. (1990) *Cell 63*, 851–859.

Baltensperger, K., Kozma, L. M., Cherniack, A. D., Klarlund, J. K., Chawla, A., Banerjee, U., & Czech, M. P. (1993) *Science 260*, 1950–1952.

Barbacid, M. (1987) *Annu. Rev. Biochem. 56*, 779–827.

Barbato, G., Ikura, M., Kay, L. E., Pastor, R. W., & Bax, A. (1992) *Biochemistry 31*, 5269–5278.

Bax, A., Clore, G. M., Driscoll, P. C., Gronenborn, A. M., Ikura, M., & Kay, L. E. (1990a) *J. Magn. Reson. 87*, 620–627.

Bax, A., Clore, G. M., & Gronenborn, A. M. (1990b) *J. Magn. Reson. 88*, 425–431.

Bax, A., Ikura, M., Kay, L. E., & Zhu, G. (1991) *J. Magn. Reson. 91*, 174–178.

Bos, J. L. (1989) *Cancer Res. 49*, 4682–4689.

Boucher, W., Laue, E. D., Campbell-Burk, S., & Domaille, P. J. (1992a) *J. Am. Chem. Soc. 114*, 2262–2264.

Boucher, W., Laue, E. D., Campbell-Burk, S., & Domaille, P. J. (1992b) *J. Biomol. NMR 2*, 631–637.

Bourne, H. R., Sanders, D. A., & McCormick, F. (1991) *Nature 349*, 117–126.

Bowtell, D., Fu, P., Simon, M., & Senior, P. (1992) *Proc. Natl. Acad. Sci. U.S.A. 89*, 6511–6515.

Bradford, M. (1976) *Anal. Biochem. 72*, 248–254.

Brooks, B. R., Bruccoleri, R. E., Olafson, B. D., States, D. J., Swaminathan, S., & Karplus, M. (1983) *J. Comput. Chem. 4*, 187–217.

Brünger, A. T. (1992) *X-PLOR Manual, Version 3.0*, Yale University, New Haven, CT.

Brünger, A. T., Milburn, M. V., Tong, L., de Vos, A. M., Jancarik, J., Yamaizumi, Z., Nishimura, S., Ohtsuka, E., & Kim, S.-H. (1990) *Proc. Natl. Acad. Sci. U.S.A. 87*, 4849–4853.

Buday, L., & Downward, J. (1993) *Cell 73*, 611–620.

Campbell-Burk, S. (1989) *Biochemistry 28*, 9478–9484.

Campbell-Burk, S., Papastavros, M. Z., McCormick, F., & Redfield, A. G. (1989) *Proc. Natl. Acad. Sci. U.S.A. 86*, 817–820.

Campbell-Burk, S. L., Domaille, P. J., Starovasnik, M. A., Boucher, W., & Laue, E. D. (1992) *J. Biomol. NMR 2*, 639–646.

Chardin, P., Camonis, J. H., Gale, N. W., Van Aelst, L., Schlessinger, J., Wigler, M. H., & Bar-Sagi, D. (1993) *Science 260*, 1338–1343.

Chung, H.-H., Benson, D. R., & Schultz, P. G. (1993) *Science 259*, 806–809.

Clore, G. M., Bax, A., Driscoll, P. C., Wingfield, P. T., & Gronenborn, A. M. (1990) *Biochemistry 29*, 8172–8184.

Clore, G. M., Kay, L. E., Bax, A., & Gronenborn, A. M. (1991) *Biochemistry 30*, 12–18.

Clowes, R. T., Boucher, W., Hardman, C. H., Domaille, P. J., & Laue, E. D. (1993) *J. Biomol. NMR 3*, 349–354.

Davis, R. J. (1993) *J. Biol. Chem. 268*, 14553–14556.

Dent, P., Haser, W., Haystead, T. A. J., Vincent, L. A., Roberts, T. M., & Sturgill, T. W. (1992) *Science 257*, 1404–1407.

Der, C. J., Pan, B.-T., & Cooper, G. M. (1986a) *Mol. Cell. Biol. 6*, 3291–3294.

Der, C. J., Finkel, T., & Cooper, G. M. (1986b) *Cell 44*, 167–176.

De Vos, A. M., Tong, L., Milburn, M. V., Matias, P. M., Jancarik, J., Noguchi, S., Nishimura, S., Miura, K., Ohtsuka, E., & Kim, S.-H. (1988) *Science 239*, 888–893.

Egan, S. E., Giddings, B. W., Brooks, M. W., Buday, L., Sizeland, A. M., & Reinberg, R. A. (1993) *Nature 363*, 45–51.

Eggenberger, U., Karimi-Nejad, Y., Thuring, H., Ruterjans, H., & Griesinger, C. (1992) *J. Biomol. NMR 2*, 583–590.

Farnsworth, C. L., & Feig, L. A. (1991) *Mol. Cell. Biol. 11*, 4822–4829.

Foley, C. K., Pedersen, L. G., Charifson, P. S., Darden, T. A., Wittinghofer, A., Pai, E. F., & Anderson, M. W. (1992) *Biochemistry 31*, 4951–4959.

Gale, N. W., Kaplan, S., Lowenstein, E. J., Schlessinger, J., & Bar-Sagi, D. (1993) *Nature 363*, 88–92.

Gibbs, J. B., Schaber, M. D., Allard, W. J., Sigal, I. S., & Scolnick, E. M. (1988) *Proc. Natl. Acad. Sci. U.S.A. 85*, 5026–5030.

Goody, R. S., Pai, E. F., Schlichting, I., Rensland, H., Scheideg, A., Franken, S., & Wittinghofer, A. (1992) *Philos. Trans. R. Soc. London, Ser. B 336*, 3–11.

Hommel, U., Harvey, T. S., Driscoll, P. C., & Campbell, I. (1992) *J. Mol. Biol. 227*, 271–282.

Howe, L. R., & Marshall, C. J. (1993) *Oncogene 8*, 2583–2590.

Howe, L. R., Leevers, S. J., Gomez, N., Nakielry, S., Cohen, P., & Marshall, C. J. (1992) *Cell 71*, 335–342.

Hughes, D. A., Ashworth, A., & Marshall, C. J. (1993) *Nature 364*, 349–352.

Hwang, Y.-W., & Miller, D. L. (1987) *J. Biol. Chem. 262*, 13081–13085.

Hyberts, S. G., Goldberg, M. S., Havel, T. F., & Wagner, G. (1992) *Protein Sci. 1*, 736–751.

Ikura, M., Kay, L. E., & Bax, A. (1990) *Biochemistry 29*, 4659–4667.

John, J., Schlichting, I., Schiltz, E., Rosch, P., & Wittinghofer, A. (1989) *J. Biol. Chem. 264*, 13086–13092.

Kay, L. E., Torchia, D. A., & Bax, A. (1989) *Biochemistry 28*, 8972–8979.

Kay, L. E., Clore, G. M., Bax, A., & Gronenborn, A. M. (1990) *Science 249*, 411–414.

Kikuchi, A., Kaibuchi, K., Hori, Y., Nonaka, H., Sakoda, T., Kawamura, M., Mizuno, T., & Takai, Y. (1992) *Oncogene 7*, 289–293.

Kraulis, P. J. (1989) *J. Magn. Reson. 84*, 627–633.

Kraulis, P. J. (1991) *J. Appl. Crystallogr. 24*, 946–950.

Krengel, U., Schlichting, I., Scherer, A., Schumann, R., Frech, M., John, J., Kabsch, W., Pai, E. F., & Wittinghofer, A. (1990) *Cell 62*, 539–548.

Kyriakis, J. M., App, H., Zhang, X.-F., Banerjee, P., Brautigan, D. L., Rapp, U. R., & Avruch, J. (1992) *Nature 358*, 417–421.

Lancelot, G., Mayer, R., & Helene, C. (1979) *J. Am. Chem. Soc. 101*, 1569–1576.

Langen, R., Schweins, T., & Warshel, A. (1992) *Biochemistry 31*, 8691–8696.

Latwesen, D. G., Poe, M., Leigh, J. S., & Reed, G. H. (1992) *Biochemistry 31*, 4946–4950.

Laue, E. D., Mayger, M. R., Skilling, J., & Staunton, J. (1986) *J. Magn. Reson. 68*, 14–29.

Li, N., Batzer, A., Daly, R., Yajnik, V., Skolnik, E., Chardin, P., Bar-Sagi, D., Margolis, B., & Schlessinger, J. (1993) *Nature 363*, 85–88.

Marion, D., Kay, L. E., Sparks, S. W., Torchia, D. A., & Bax, A. (1989a) *J. Am. Chem. Soc. 111*, 1515–1517.

Marion, D., Driscoll, P. C., Kay, L. E., Wingfield, P. T., Bax, A., Gronenborn, A. M., & Clore, G. M. (1989b) *Biochemistry 28*, 6150–6156.

Marion, D., Ikura, M., & Bax, A. (1989c) *J. Magn. Reson. 84*, 425–430.

Marshall, M. (1993) *Trends Biochem. Sci. 18*, 250–254.

Martegani, E., Vanoni, M., Zippel, R., Coccetti, P., Brambilla, R., Farrari, C., Sturani, E., & Albergina, L. (1992) *EMBO J. 11*, 2151–2157.

Martin, G. A., Viskochil, D., Bollag, G., McCabe, P. C., Crosier, W. J., Haubruck, H., Conroy, L., Clark, R., O'Connell, P., Cawthon, R. M., Innis, M. A., & McCormick, F. (1990) *Cell 63*, 843–849.

Milburn, M. V., Tong, L., de Vos, A. M., Brunger, A., Yamaizumi, Z., Nishimura, S., & Kim, S.-H. (1990) *Science 247*, 939–945.

Mistou, M.-V., Jacquet, E., Poullet, P., Rensland, H., Gideon, P., Schlichting, I., Wittinghofer, A., & Parmeggiani, A. (1992) *EMBO J. 11*, 2391–2397.

Moodie, S. A., Willumsen, B. M., Weber, M. J., & Wolfman, A. (1993) *Science 260*, 1658–1661.

Muto, Y., Yamasaki, K., Ito, Y., Yajima, S., Masaki, Y., Uozumi, T., Walchli, M., Nishimura, S., Miyazawa, T., & Yokoyama, S. (1993) *J. Biomol. NMR 3*, 165–184.

Nilges, M., Gronenborn, A. M., Brünger, A. T., & Clore, G. M. (1988) *Protein Eng. 2*, 27–38.

Olivier, J. P., Raabe, T., Henkemyer, M., Dickson, B., Mbamalu, G., Margolis, B., Schlessinger, J., Hafen, E., & Pawson, T. (1993) *Cell 73*, 179–191.

Pai, E. F., Kabsch, W., Krengel, U., Holmes, K. C., John, J., & Wittinghofer, A. (1989) *Nature 341*, 209–214.

Pai, E. F., Krengel, U., Petsko, G. A., Goody, R. S., Kabsch, W., & Wittinghofer, A. (1990) *EMBO J. 9*, 2351–2359.

Prive, G. G., Milburn, M. V., Tong, L., de Vos, A. M., Yamaizumi, Z., Nishimura, S., & Kim, S.-H. (1992) *Proc. Natl. Acad. Sci. U.S.A. 89*, 3649–3653.

Rance, M. (1987) *J. Magn. Reson. 74*, 557–564.

Redfield, A. G., & Papastavros, M. Z. (1990) *Biochemistry 29*, 3509–3514.

Richardson, J. M., Clowes, R. T., Boucher, W., Domaille, P. J., Hardman, C. H., Keeler, J., & Laue, E. D. (1993) *J. Magn. Reson., Ser. B 101*, 223–227.

Rozakis-Adcock, M., Fernley, R., Wade, J., Pawson, T., & Bowdell, D. (1993) *Nature 363*, 83–85.

Schlichting, I., Almo, S. C., Rapp, G., Wilson, K., Petratos, K., Lentfer, A., Wittinghofer, A., Kabsch, W., Pai, E. F., Petsko, G. A., & Goody, R. S. (1990a) *Nature 345*, 309–315.

Schlichting, I., John, J., Frech, M., Chardin, P., Wittinghofer, A., Zimmermann, H., & Rosch, P. (1990b) *Biochemistry 29*, 504–511.

Shaka, A. J., Lee, C. J., & Pines, A. (1988) *J. Magn. Reson. 77*, 274–293.

Shirakawa, M., Fairbrother, W. J., Serikawa, Y., Ohkubo, T., Kyoguko, Y., & Wright, P. E. (1993) *Biochemistry 32*, 2144–2153.

Shou, C., Farnsworth, C. L., Neel, B. G., & Feig, L. A. (1992) *Nature 358*, 315–334.

Simon, M. A., Dodson, G. S., & Rubin, G. M. (1993) *Cell 73*, 169–177.

Skolnik, E. Y., Batzer, A., Li, N., Lee, C.-H., Lowenstein, E., Mohammadi, M., Margolis, M., & Schlessinger, J. (1993) *Science 260*, 1953–1955.

Stouten, P. F. W., Sander, C., Wittinghofer, A., & Valencia, A. (1993) *FEBS Lett. 320*, 1–6.

Tong, L., Milburn, M. V., de Vos, A. M., & Kim, S.-H. (1989) *Science 245*, 244.

Tong, L., de Vos, A. M., Milburn, M. V., & Kim, S.-H. (1991) *J. Mol. Biol. 217*, 503–516.

Trahey, M., & McCormick, F. (1987) *Science 238*, 542–545.

Tucker, J., Sezakiel, G., Feuerstein, J., John, J., Goody, R. S., & Wittinghofer, A. (1986) *EMBO J. 5*, 1351–1358.

Van Aelst, L., Barr, M., Marcus, S., Polverino, A., & Wigler, M. (1993) *Proc. Natl. Acad. Sci. U.S.A. 90*, 6213–6217.

Verrotti, A. C., Crechet, J. B., Di Blasi, F., Seidita, G., Mirisola, M. G., Kavounis, C., Nastopoulos, V., Burderi, E., De Vendittis, E., Parmeggiani, A., & Fasano, O. (1992) *EMBO J. 11*, 2855–2862.

Vojtek, A. B., Hollenberg, S. M., & Cooper, J. A. (1993) *Cell 74*, 205–214.

Warne, P. H., Viciana, P. R., & Downward, J. (1993) *Nature 364*, 352–355.

Wei, W., Mosteller, R. D., Sanyal, P., Gonzales, E., McKinney, D., Dasgupta, C., Li, P., Liu, B.-X., & Broek, D. (1992) *Proc. Natl. Acad. Sci. U.S.A. 89*, 7100–7104.

Willumsen, B. M., Vass, W. C., Velu, T. J., Papageorge, A. G., Schiller, J. T., & Lowy, D. R. (1991) *Mol. Cell. Biol. 11*, 6026–6033.

Wüthrich, K., Billeter, M., & Braun, W. (1983) *J. Mol. Biol. 169*, 949–961.

Xu, G. F., O'Connell, P., Viskochil, D., Cawthon, R., Robertson, M., Culver, M., Dunn, D., Stevens, J., Gesteland, R., White, R., & Weiss, R. (1990) *Cell 62*, 599–608.

Yamasaki, K., Kawai, G., Ito, Y., Muto, Y., Fujita, J., Miyazawa, T., Nishimura, S., & Yokoyama, S. (1989) *Biochem. Biophys. Res. Commun. 162*, 1054–1062.

Yamasaki, K., Muto, Y., Ito, Y., Walchli, M., Miyazawa, T., Nishimura, S., & Yokoyama, S. (1992) *J. Biomol. NMR 2*, 71–82.

Zhang, X.-F., Settleman, J., Kyriakis, J. M., Takeuchi-Suzuki, E., Elledge, S. J., Marshall, M., Bruder, J. T., Rapp, U. R., & Avruch, J. (1993) *Nature 364*, 308–313.

Zuiderweg, E. R. P., Boelens, R., & Kaptein, R. (1985) *Biopolymers 24*, 601–611.

Zuiderweg, E. R. P., McIntosh, L. P., Dahlquist, F. W., & Fesik, S. W. (1990) *J. Magn. Reson. 86*, 210–216.

Zuiderweg, E. R. P., Petros, A. M., Fesik, S. W., & Olejniczak, E. T. (1991) *J. Am. Chem. Soc. 113*, 370–372.